Iran J Sci Technol Trans Mech Eng (2019) 43:457–475
https://doi.org/10.1007/s40997-018-0220-7

RESEARCH PAPER

Thermo-Elastic Column Buckling of Tapered Nanowires with Axially Varying Material Properties: A Critical Study on the Roles of Shear and Surface Energy

Keivan Kiani[1]

Received: 9 March 2017 / Accepted: 9 July 2018 / Published online: 16 July 2018

Abstract
At the nanoscale, shear and surface energy play important roles in mechanical behavior of nanostructures, and therefore, such effects should be appropriately considered in the corresponding structural modeling. Herein, surface energy-based Euler–Bernoulli, Timoshenko, and higher-order beam theories are implemented to study buckling of thermally affected tapered nanowires with axial variation of materials. The governing equations associated with thermo-elastic buckling of nanowires are derived for an arbitrary variation of material properties of both bulk and surface layer across the length of nanostructure. In the lack of analytical solution, reproducing kernel particle method is adopted and the critical buckling load is evaluated. The effects of temperature gradient, slenderness ratio, power-law index of the material and geometry of the nanowire, radius, as well as transverse and rotational stiffness of the surrounding elastic medium on the buckling behavior of the nanowire are investigated. The importance of consideration of both surface energy and shear deformation effects on the obtained results is also highlighted. This work could be taken into account as a preliminary research in examining buckling of more complex nanosystems such as vertically aligned nanowires with arbitrary material's distribution and cross section.

Keywords Thermo-elastic buckling · Tapered nanowires · Elasticity theory of Gurtin–Murdoch · Shear deformable beam theories · Numerical modeling

1 Introduction

A nanowire is a nanostructure of thickness or diameter about tens of nanometers or less and of large amount of the length-to-width ratio. To date, various types of nanowires have been synthesized, including metallic (e.g., Au, Cu, Ag, Ni, Pt, Al) (Kwak et al. 2016; Nunes et al. 2016), semiconducting (e.g., Si, GaN, ZnO, InP) (Ruffino et al. 2015; Tao et al. 2015; Srivastava et al. 2016), superconducting (e.g., NbN, BSCCO, YBCO) (Korneev et al. 2012; Duarte et al. 2013), molecular nanowires with organic or inorganic molecules [e.g., DNA or $(C_6H_{14}N)_2$] (Mousavi et al. 2015; Lin et al. 2014), and insulating (e.g., TiO_2 or SiO_2) (Ahn et al. 2015; Tang et al. 2015). These nanowires would have great applications in energy harvesting, dye-sensitized solar cells, mechanical sensing, photon detection, electronics, and as resonators. Nowadays, scientists are thinking to exploit arrays of nanowires as building blocks of the upcoming advanced technologies of nanogenerators (Wang et al. 2007; Zhu et al. 2010; Xu et al. 2010) as well as micro-/nanoelectromechanical systems (MEMS/NEMS) (Shi et al. 2005; Hochbaum et al. 2005; Patton and Zabinski 2005). Nanowires are also of particular interest to be exploited for enhancing flow boiling heat transfer (Chen et al. 2009; Li et al. 2012a; Lu et al. 2011), carrying safe heat flux in transistors (Pop et al. 2006), and managing heat in electronic nanodevices (Schelling et al. 2005). In most of these potential applications, the axial load-bearing capacity of heated nanowires should be carefully investigated.

✉ Keivan Kiani
k_kiani@kntu.ac.ir; keivankiani@yahoo.com

[1] Department of Civil Engineering, K.N. Toosi University of Technology, P.O. Box 15875-4416, Valiasr Ave., Tehran, Iran

As the dimensions of a structure decrease, the ratio of the surface strain energy to that of the bulk would grow. Thereby, at the nanoscale, the effect of the surface energy on the overall mechanical behavior of the nanostructure becomes important. In macrostructures, the surface effect is negligible and the classical elasticity theory (CET) could be rationally employed for predicting their statics, dynamical, and buckling behaviors. However, there exist evidences that this theory fails in capturing the near to exact mechanical behavior of nanowires (Cuenot et al. 2004; Jing et al. 2006; Gordon et al. 2009). As an approach to conquer this deficiency of the CET, Gurtin and Murdoch (Gurtin and Murdoch 1975, 1976) proposed a novel theory of elasticity to appropriately include energy of surface atoms. Based on this elegantly developed model, the surface is a very thin layer which has been perfectly attached to the bulk. It is indicated that the displacements and strains of the surface layer are identical to those of the neighboring bulk. However, the mechanical behavior of the surface layer is entirely different from that of the bulk. The strain–stress relations of the surface layer of isotropic structures are commonly characterized by three constants (i.e., residual surface stress as well as two Lame's constants), whereas those of the isotropic bulk are governed by only two Lame's constants associated with the bulk. Such a fact does not make the resulting governing equations more complex than those obtained via the CET. Factually, including the surface layer only leads to insertion of extra terms to the inertia and stiffness terms of the bulk. Concerning mechanical behavior of beam-like nanostructures, transverse vibrations (Hasheminejad et al. 2011; Kiani 2016a), elastic buckling (Wang and Feng 2009, 2010; Xiao et al. 2010; Park 2012; Kiani 2015a, b, 2016b, c; Chiu and Chen 2012; Ansari et al. 2011), and postbuckling (Li et al. 2011; Wang and Yang 2011; Li et al. 2012b; Ansari et al. 2013; Kiani 2017a) of nanowires and nanobeams have been studied in the context of the SET of Gurtin–Murdoch. Additionally, nonlocal continuum field theory in conjunction with the SET has been also employed for buckling analysis of several nanoscaled structures (Lee and Chang 2011; Wang and Wang 2011; Juntarasaid et al. 2012; Farajpour et al. 2013; Hu et al. 2014; Kiani 2017b).

One way to reduce the stresses within a thermally affected nanobeam is to use an appropriate mixture of materials across the length. In fact, if we could exploit materials whose coefficients of thermal expansion as well as those of thermal conductivity would gradually reduce by approaching to the heat source, lower stresses would be generated within the nanobeam, and therefore, the nanostructure could bear a more axial load. There are many experimental works in building structures at the nanoscale with functional materials for various purposes (Barth et al. 2005; Yang et al. 2008; Matyjaszewski and Tsarevsky 2009; Cheng et al. 2011). In general, it can be imagined that the properties of the materials in a nanobeam could vary along its length and across its thickness. Since providing nanoscaled structures with variation of materials in both directions is not an easy task, the material properties are allowed to gradually change along a special direction according to the required functionality from the nanostructure. Based on this fact, buckling of nanobeams made from transversely functionally graded materials (Simsek and Yurtcu 2013; Eltaher et al. 2013) has been examined using advanced continuum-based theories. Nevertheless, Thermo-elastic buckling of nanoscaled beam-like structures with axially functionally graded materials has not been discussed and formulated yet. Given the importance of the subject, this work is devoted to study axial buckling of thermally affected nanobeam with allowance of material variation across the length.

Using surface elasticity theory of Gurtin–Murdoch, thermo-elastic buckling of tapered nanowires/nanobeams with axially varying material embedded within an elastic matrix, hereinafter called *axially varying nanowires* (AVNWs), is going to be investigated. Based on the Euler–Bernoulli beam theory (EBT), Timoshenko beam theory (TBT), and higher-order beam theory (HOBT), the governing equations are constructed. To solve the resulting relations, reproducing kernel particle method (RKPM) is exploited and the critical buckling load of the thermally affected nanostructure based on various beam models is evaluated. By comparing the predicted results by the RKPM and those of the Galerkin-based assumed mode method (AMM), the efficiency of the suggested numerical scheme is proved. Subsequently, the roles of influential factors on the predicted critical buckling load are explained. The discrepancies between the obtained results based on the classical elasticity theory (CET) and those of the surface elasticity theory (SET) are also displayed and discussed. This work, with its own generality in buckling analysis of individual nanowires with axially varying materials, can be considered as a pivotal exploration for buckling analysis of double-nanowire systems or even vertically aligned nanowires in thermal environments. These hot topics could be followed up by the interested researchers since the latter one would have great applications in MEMS/NEMS.

2 Definition and Assumptions of the Nanomechanical Problem

Consider an elastic non-prismatic nanowire/nanobeam of length l_b whose material properties vary gradually along its length (see Fig. 1). The nanowire has circular cross section whose the diameter of the bulk is represented by $D_0(x)$.

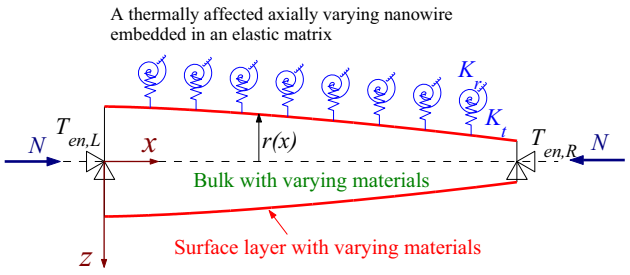

Fig. 1 A thermally affected tapered nanowire with axially varying material subjected to thermo-mechanical axial force

The nanowire is prohibited from any axial movement at its ends and it is subjected to axial compressive load of magnitude N as well as the axial thermal field $T = T(x)$. Evaluation of the axial load corresponding to the buckling of such a nanostructure (i.e., N_{cr}) is of concern in the present work. In order to model the nanostructure, the following assumptions are made:

1. The buckling behavior of the nanostructure under the action of both the axial load and the induced thermal field is studied in the context of elastic small deflection. In other words, only thermo-elastic buckling analysis of the nanowire is of concern. For the postbuckling analysis of the nanowire, one confronts to a large deflection problem and special treatments should be considered in modeling of the problem.
2. The material properties of materials only vary across the length of the nanowire. For nanowires with bidirectionally varying materials, more refined models should be constructed. For instance, in the case of variation of material properties across the transverse direction, the neutral axis of the beam-like nanowire would not necessarily pass through the center of cross-sectional area.
3. The heat transfer occurs axially due to the existence of steady temperature gradient between the ends of the nanowire. Thereby, the resulted temperature field only varies across the axial direction. It implies that a steady axially thermo-mechanical force would be generated within the nanowire. For the case of transverse heat transfer, thermo-mechanical bending moment would be also generated within the nanowire. Additionally, when the temperature of the nanowire's ends is time dependent, an unsteady temperature resulted in the body of the nanowire and the generated axial force would be time dependent as well. Such more general cases could be considered for future works.
4. The possible lateral interactions between the nanowire and the surrounding elastic medium are modeled by continuous transverse and rotational springs. Generally, the constants of these springs could vary along the nanowire's length and depend on the material properties of both nanowire and matrix as well as their interatomic bonds. Without loss of generality, to focus on the roles of variation of cross section and material properties of the nanowire in the critical buckling load, the variation of the springs' constants across the nanowire's length is ignored. In all presented models, the constants of the transverse and rotational springs are considered to be K_t and K_r, respectively.

In the next part, the governing equations associated with thermo-elastic buckling of nanowires/nanobeams with varying cross section are presented based on the EBT, TBT, and HOBT. For each developed model, a numerical methodology based on the RKPM is developed and the critical compressive buckling load of the nanostructure is determined.

3 Axially Thermo-Elastic Buckling Based on the Surface Energy-Based EBT

3.1 Governing Equations Using the EBT

According to the EBT, the displacement fields of both bulk and the surface layer read:

$$u_x^E(x,y,z) = -z\frac{\mathrm{d}w^E(x)}{\mathrm{d}x}, \quad u_z^E(x,y,z) = w^E(x), \tag{1}$$

where u_x^E and u_z^E in order are the axial and transverse displacements of the nanowire, $w^E(x)$ is the deflection of the neutral axis of the nanowire, and d stands for the derivative symbol. Thereby, the only nonzero strain within the bulk would be:

$$\epsilon_{xx}^E = -z\frac{\mathrm{d}^2w^E(x)}{\mathrm{d}x^2}. \tag{2}$$

In the context of the surface elasticity theory of Gurtin–Murdoch (Gurtin and Murdoch 1975, 1976), the only nonzero stresses within the surface layer are as:

$$\begin{aligned}\tau_{xx}^E &= \tau_0(x) + (\lambda_0(x) + 2\mu_0(x))\frac{\mathrm{d}u_x^E}{\mathrm{d}x}\\ &= \tau_0(x) - z\,(\lambda_0(x) + 2\mu_0(x))\frac{\mathrm{d}^2w^E}{\mathrm{d}x^2},\\ \tau_{xz}^E &= n_z\tau_0(x)\frac{\mathrm{d}w^E}{\mathrm{d}x},\end{aligned} \tag{3}$$

where τ_{xx}^E is the surface axial stress, τ_{xz}^E is the surface shear stress, τ_0 is the residual surface stress under unconstrained conditions, λ_0 and μ_0 are the axially varying Lame's

constants of the surface layer, and $\mathbf{n} = n_y\mathbf{e}_y + n_z\mathbf{e}_z$ is the unit normal vector of the surface layer.

It is assumed that the bulk normal stress along the z-axis (i.e., σ^E_{zz}) would vary linearly between their surface values at the bottom and top axes. Thereby,

$$\sigma^E_{xx} = E_b\epsilon^E_{xx} + v_b\,\sigma^E_{zz} = -z\left(E_b(x) - \frac{2\tau_0(x)v_b(x)}{D_0(x)}\right)\frac{\mathrm{d}^2w^E}{\mathrm{d}x^2}, \tag{4}$$

where $\rho_0(x)$ is the surface density, $E_b(x)$ and $v_b(x)$ in order are the spatially varying Young's modulus and Poisson's ratio of the bulk.

By taking an infinitesimal element of the nanowire, considering all the forces act on the bulk and the surface layer, and using Newton's second law, the governing equations associated with the elastic buckling of the thermally affected AVNW are obtained as follows:

$$-\frac{\mathrm{d}M^E_{b_y}}{\mathrm{d}x} - \int_{\mathcal{S}} z\,\frac{\mathrm{d}\tau^E_{xx}}{\mathrm{d}x}\,\mathrm{d}\mathcal{S} + Q^E_{b_z} - K_r\frac{\mathrm{d}w^E}{\mathrm{d}x} = 0, \tag{5a}$$

$$-\frac{\mathrm{d}Q^E_{b_z}}{\mathrm{d}x} - \int_{\mathcal{S}} \frac{\mathrm{d}\tau^E_{xz}}{\mathrm{d}x}n_z\,\mathrm{d}\mathcal{S} + (N - N_T)\,\frac{\mathrm{d}^2w^E}{\mathrm{d}x^2} + K_t w^E = 0, \tag{5b}$$

where $\mathrm{d}\mathcal{S}$ is the length of a tiny element of the surface layer's cross section, $Q^E_{b_z}$ is the resultant shear force of the bulk, and N_T represents the resulted axial force in the nanostructure due to the thermal field.

For a nanowire in which the environmental temperatures at the left and right ends are denoted by $T_{en,L}$ and $T_{en,R}$, the temperature field within the nanowire is calculated by:

$$T(\xi) = \left[\frac{\chi_{22}\Gamma_1 - \chi_{12}\Gamma_2}{\chi_{22}\chi_{11} - \chi_{12}\chi_{21}}\right]\int_0^{\xi}\frac{\mathrm{d}\xi'}{k(\xi')} + \left[\frac{\chi_{11}\Gamma_2 - \chi_{21}\Gamma_1}{\chi_{22}\chi_{11} - \chi_{12}\chi_{21}}\right], \tag{6}$$

where

$$\begin{aligned}
&\xi = \frac{x}{l_b}, \quad \beta_L = \frac{h_L\,l_b}{k_L}, \quad \beta_R = \frac{h_R\,l_b}{k_R}, \quad \chi_{11} = -\frac{1}{k_L},\\
&\chi_{12} = \beta_L, \quad \chi_{21} = \beta_R\int_0^1\frac{\mathrm{d}\xi'}{k(\xi')} - \frac{1}{k_R}, \quad \chi_{22} = \beta_R,\\
&\Gamma_1 = \beta_L\,T_{en,L}, \quad \Gamma_2 = \beta_R\,T_{en,R},
\end{aligned} \tag{7}$$

in which $k(x)$, k_L, and k_R represent the coefficients of thermal conductivity of the nanobeam's materials, the left end, and the right end, respectively, h_L and h_R in order denote the heat transfer coefficients of the left end and the right end of the nanostructure.

It could be readily researched that the thermally axial force within the nanowire accounting for the surface effect is expressed by:

$$N_T = -\int_0^1 \left(E_b(\xi)A_b(\xi)\alpha_T(\xi) + E_0(\xi)S_0(\xi)\alpha_{T0}(\xi)\right)T(\xi)\,\mathrm{d}\xi, \tag{8}$$

where $E_0(x)$ and $E_b(x)$ in order are Young's modulus of the surface layer and the bulk, $\alpha_T(x)$ and $\alpha_{T0}(x)$ denote the coefficients of thermal expansion of the bulk and the surface layer, respectively, $A_b(x)$ denotes the cross-sectional area of the bulk, and $S_0(x)$ is the length of surface layer's cross section.

In Eq. (5), $M^E_{b_y}$ is the resultant bending moment of the bulk about the y-axis which is given by:

$$\begin{aligned}
M^E_{b_y} &= \int_{A_b} z\sigma^E_{xx}\,\mathrm{d}A\\
&= -\left(E_b(x)I_b(x) - \frac{2\tau_0(x)v_b(x)I_b(x)}{D_0(x)}\right)\frac{\mathrm{d}^2w^E}{\mathrm{d}x^2}.
\end{aligned} \tag{9}$$

where A_b represents the area of the bulk's cross section, $\mathrm{d}A$ is its infinitesimal part, and $I_b(x)$ is the moment inertia of the bulk's cross section. By mixing Eqs. (5a) and (5b) in view of Eq. (9) through using the following dimensionless quantities,

$$\begin{aligned}
&\overline{w}^E = \frac{w^E}{l_b}, \quad \lambda = \frac{l_b}{r_{b,L}}, \quad \overline{A}_b(\xi) = \frac{A_b(x)}{A_{b,L}}, \quad \overline{I}_b(\xi) = \frac{I_b(x)}{I_{b,L}},\\
&\overline{N}^E = \frac{Nl_b^2}{E_{b,L}I_{b,L}}, \quad \overline{N}^E_T = \frac{N_Tl_b^2}{E_{b,L}I_{b,L}}, \quad \overline{K}^E_t = \frac{K_tl_b^4}{E_{b,L}I_{b,L}},\\
&\overline{K}^E_r = \frac{K_rl_b^2}{E_{b,L}I_{b,L}}, \quad \chi^E_1(\xi) = \frac{\rho_0(x)S^*_0(x)}{\rho_{b,L}A_{b,L}},\\
&\chi^E_2(\xi) = \frac{\rho_0(x)I^*_0(x) - \frac{2v_b(x)I_b(x)\rho_0(x)}{D_0(x)}}{\rho_{b,L}I_{b,L}},\\
&\chi^E_3(\xi) = \frac{(\lambda_0(x) + 2\mu_0(x))I^*_0(x) - \frac{2v_b(x)I_b(x)\tau_0(x)}{D_0(x)}}{E_{b,L}I_{b,L}},\\
&\chi^E_4(\xi) = \frac{\tau_0(x)S^*_0(x)l_b^2}{E_{b,L}I_{b,L}},
\end{aligned} \tag{10}$$

where $r_{b,L}$, $A_{b,L}$, $I_{b,L}$, $\rho_{b,L}$, and $E_{b,L}$ are the gyration radius, area, moment inertia, bulk's density, and Young's modulus of the bulk of the left end's cross section, respectively. By introducing Eqs. (10) to (5) and using Eq. (9), the dimensionless governing equation of the column buckling of thermally affected nanostructure based on the EBT takes the following form:

$$\begin{aligned}
&\frac{\mathrm{d}^2}{\mathrm{d}\xi^2}\left[\left(\overline{E}_b(\xi)\overline{I}_b(\xi) + \chi^E_3(\xi)\right)\frac{\mathrm{d}^2\overline{w}^E}{\mathrm{d}\xi^2}\right]\\
&\quad - \left(\chi^E_4(\xi) + \overline{N}^E_T + \overline{K}^E_r - \overline{N}^E\right)\frac{\mathrm{d}^2\overline{w}^E}{\mathrm{d}\xi^2} + \overline{K}^E_t\,\overline{w}^E = 0.
\end{aligned} \tag{11}$$

Due to the variation of both geometry and material properties along the length of the nanowire, finding an

analytical solution to Eq. (11) is not an easy task. In the following part, an efficient numerical scheme is proposed to determine the critical buckling load of the nanowire.

3.2 Thermo-Elastic Buckling Analysis of the EBT-Based Nanowire via RKPM

RKPM is an efficient meshless methodology that was developed by Liu and coworkers (Liu et al. 1995a, b; Liu and Chen 1995) about twenty years ago. Commonly, this method is employed for solving the mechanical/physical problems that suffer from shooting (i.e., high stress variations, high gradients of the physical fields), and those with the unknown fields of higher-order derivatives. Until now, this approach has been broadly implemented in mechanical analysis of structures (Chen et al. 1996; Wang and Liu 2004; Jun et al. 1998; Liu and Jun 1998). This is mainly because of this fact that the shape functions of this numerical method are constructed based on the window functions with higher-order of continuity.

Now the deflection of the nanowire modeled on the basis of the EBT is discretized in the following form:

$$\overline{w}^E(\xi) = \sum_{i=1}^{\mathrm{NP}} \phi_i^w(\xi)\overline{w}_i^E, \tag{12}$$

where NP is the number of RKPM's particles, $\phi_i^w(\xi)$ is the shape function pertinent to the ith particle of the dimensionless field $\overline{w}^E$, and $\overline{w}_i^E$ is the corresponding nodal parameter value of the ith particle. By pre-multiplying both sides of Eq. (11) by $\delta\overline{w}^E$, in which δ is the variation symbol, taking the integral in the spatial interval [0,1], and exploiting integration by parts, the following set of linear equations are obtained as:

$$\left([\overline{\mathbf{K}}_b^E]^{ww} - [\overline{\mathbf{K}}_g^E]^{ww}\right)\overline{\mathbf{w}}^E = \mathbf{0}, \tag{13}$$

where the nonzero elements of the thermo-material stiffness matrix and those of dimensionless geometry stiffness matrix are defined by:

$$\left[\overline{\mathbf{K}}_b^E\right]_{ij}^{ww} = \int_0^1 \begin{pmatrix} \left(\overline{E}_b(\xi)\overline{I}_b(\xi) + \chi_3^E(\xi)\right)\dfrac{\mathrm{d}^2\phi_i^w}{\mathrm{d}\xi^2}\dfrac{\mathrm{d}^2\phi_j^w}{\mathrm{d}\xi^2} \\ +\left(\chi_4^E(\xi) + \overline{N}_T^E + \overline{K}_r^E\right)\dfrac{\mathrm{d}\phi_i^w}{\mathrm{d}\xi}\dfrac{\mathrm{d}\phi_j^w}{\mathrm{d}\xi} + \overline{K}_t^E\,\phi_i^w\,\phi_j^w \end{pmatrix}\mathrm{d}\xi, \tag{14a}$$

$$\left[\overline{\mathbf{K}}_g^E\right]_{ij}^{ww} = \overline{N}^E\int_0^1 \frac{\mathrm{d}\phi_i^w}{\mathrm{d}\xi}\frac{\mathrm{d}\phi_j^w}{\mathrm{d}\xi}\,\mathrm{d}\xi, \tag{14b}$$

$$\overline{\mathbf{w}}^E = <\overline{w}_1^E, \overline{w}_2^E, \ldots, \overline{w}_{\mathrm{NP}}^E>^{\mathrm{T}}. \tag{14c}$$

For nanowires with simply supported ends, the following boundary conditions in the dimensionless manner should be enforced:

$$\overline{w}^E(0) = \overline{w}^E(1) = 0; \quad \overline{M}_{b_y}^E(0) = \overline{M}_{b_y}^E(1) = 0, \tag{15}$$

where $\overline{M}_{b_y}^E = \frac{M_{b_y}^E l_b}{E_{b,L}I_{b,L}}$. In order to satisfy the essential boundary conditions from all conditions in Eq. (15), the corrected collocation method (Wagner and Liu 2000) is used. By solving the resulting set of eigenvalue equations for the dimensionless axial buckling loads, $\overline{N}_{\mathrm{cr},i}^E$, the critical compressive buckling load of the thermally affected nanowire based on the EBT is calculated by: $N_{\mathrm{cr}}^E = \overline{N}_{\mathrm{cr},1}^E E_{b,L}I_{b,L}l_b^{-2}$ where $\overline{N}_{\mathrm{cr},1}^E$ denotes the lowest value of the obtained dimensionless buckling loads.

4 Axially Thermo-Elastic Buckling Based on the Surface Energy-Based TBT

4.1 Governing Equations Using the TBT

In the framework of TBT, the axial displacement (u_x^T) and the transverse displacement (u_z^T) of the thermally affected nanowire are related to the deformations of the neutral axis by the following relations:

$$u_x^T(x,y,z) = -z\theta_y^T(x), \quad u_z^T(x,y,z) = w^T(x), \tag{16}$$

where w^T is the deflection field of the neutral axis, and θ_y^T represents its angle of rotation field. Hence, the only nonzero strains of both bulk and surface are:

$$\epsilon_{xx}^T = -z\frac{\mathrm{d}\theta_y^T}{\mathrm{d}x}, \quad \gamma_{xz}^T = \frac{\mathrm{d}w^T}{\mathrm{d}x} - \theta_y^T. \tag{17}$$

Based on the proposed surface elasticity theory by Gurtin–Murdoch (Gurtin and Murdoch 1975, 1976), the stresses of the surface layer of the axially varying nanowire modeled on the basis of the TBT are expressed by:

$$\begin{aligned} \tau_{xx}^T &= \tau_0(x) + (\lambda_0(x) + 2\mu_0(x))\frac{\mathrm{d}u_x^T}{\mathrm{d}x} \\ &= \tau_0(x) - z\,(\lambda_0(x) + 2\mu_0(x))\,\frac{\mathrm{d}\theta_y^T}{\mathrm{d}x}, \\ \tau_{xz}^T &= n_z\tau_0\frac{\mathrm{d}w^T}{\mathrm{d}x}. \end{aligned} \tag{18}$$

By assuming linear variation of the normal stress of the bulk between their surface counterparts along the z-axis (i.e., σ_{zz}^T), the axial stress in the bulk takes the following form:

$$\sigma_{xx}^T = z\left(-E_b(x)\frac{\mathrm{d}\theta_y^T}{\mathrm{d}x} + \frac{2\nu_b(x)\tau_0(x)}{D_0(x)}\frac{\mathrm{d}^2w^T}{\mathrm{d}x^2}\right), \tag{19}$$

and the shear stress within the bulk is given by:

$$\sigma_{xz}^{T} = G_b(x)\left(\frac{\mathrm{d}w^{T}}{\mathrm{d}x} - \theta_y^{T}\right). \tag{20}$$

where $G_b(x) = \frac{E_b(x)}{2(1+\nu(x))}$ represents the shear elastic modulus. The governing equations of a beam-like nanostructure modeled based on the TBT in terms of its internal forces are given by:

$$-\frac{\mathrm{d}M_{b_y}^{T}}{\mathrm{d}x} - \frac{\mathrm{d}}{\mathrm{d}x}\left[\underline{\int_{\mathcal{S}} z\,\tau_{xx}^{T}\,\mathrm{d}\mathcal{S}}\right] + Q_{b_z}^{T} + K_r\theta_y^{T} = 0, \tag{21a}$$

$$-\frac{\mathrm{d}Q_{b_z}^{T}}{\mathrm{d}x} - \frac{\mathrm{d}}{\mathrm{d}x}\left[\underline{\int_{\mathcal{S}} \tau_{xz}^{T} n_z\,\mathrm{d}\mathcal{S}}\right] + \left(N - N_T - \tau_0(x)S_0^{*}(x)\right) \frac{\mathrm{d}^2 w^{T}}{\mathrm{d}x^2} + K_t w^{T} = 0, \tag{21b}$$

where the underlined statements in Eqs. (21a) and (21b) in order represent the bending moment and the shear force of the surface layer, $Q_{b_z}^{T}$ is the shear force of the bulk along the z-axis, and $M_{b_y}^{T}$ is the bending moment of the bulk about the y-axis which are evaluated by the following relations:

$$\begin{aligned} M_{b_y}^{T} &= \int_{A_b(x)} z\sigma_{xx}^{T}\,\mathrm{d}A \\ &= -E_b(x)I_b(x)\frac{\mathrm{d}\theta_y^{T}}{\mathrm{d}x} \\ &\quad + \frac{2\nu_b(x)I_b(x)}{D_0(x)}\left(\tau_0(x)\frac{\mathrm{d}^2 w^{T}}{\mathrm{d}x^2} - \rho_0(x)\frac{\mathrm{d}^2 w^{T}}{\mathrm{d}t^2}\right), \end{aligned} \tag{22a}$$

$$Q_{b_z}^{T} = \int_{A_b(x)} k_s(x)\,\sigma_{xz}^{T}\,\mathrm{d}A = k_s(x)G_b(x)A_b(x)\left(\frac{\mathrm{d}w^{T}}{\mathrm{d}x} - \theta_y^{T}\right), \tag{22b}$$

where $k_s(x)$ denotes the shear correction factor which is set equal to 0.9 for nanowires with circular cross section. Through introducing Eqs. (16), (18), (22a), and (22b) to Eqs. (21a)–(21d), and employing the following dimensionless quantities:

$$\begin{aligned} &\overline{w}^{T} = \frac{w^{T}}{l_b}, \quad \overline{\theta}_y^{T} = \theta_y^{T}, \quad \overline{k}_s(\xi) = \frac{k_s(x)}{k_{s,L}}, \\ &\overline{G}_b(\xi) = \frac{G_b(x)}{G_{b,L}}, \quad \overline{K}_t^{T} = \frac{K_t l_b^2}{k_{s,L}G_{b,L}A_{b,L}}, \\ &\overline{K}_r^{T} = \frac{K_r}{k_{s,L}G_{b,L}A_{b,L}}, \quad \eta(\xi) = \frac{E_b(x)I_b(x)}{k_{s,L}G_{b,L}A_{b,L}l_b^2}, \\ &\overline{N}^{T} = \frac{N}{k_{s,L}G_{b,L}A_{b,L}}, \quad \overline{N}_T^{T} = \frac{N_T}{k_{s,L}G_{b,L}A_{b,L}}, \\ &\chi_1^{T}(\xi) = \frac{\rho_0(x)S_0^{*}(x)}{\rho_{b,L}A_{b,L}}, \\ &\chi_2^{T}(\xi) = \frac{\rho_0(x)I_0^{*}(x)}{\rho_{b,L}I_{b,L}}, \quad \chi_3^{T}(\xi) = \frac{2\nu_b(x)\rho_0(x)}{\rho_{b,L}D_0(x)}, \\ &\chi_4^{T}(\xi) = \frac{2\nu_b(x)I_b(x)\tau_0(x)}{k_{s,L}G_{b,L}A_{b,L}l_b^2 D_0(x)}, \\ &\chi_5^{T}(\xi) = \frac{(\lambda_0(x)+2\mu_0(x))I^{*}(x)}{k_{s,L}G_{b,L}A_{b,L}l_b^2}, \quad \chi_6^{T}(\xi) = \frac{\tau_0(x)S_0^{*}(x)}{k_{s,L}G_{b,L}A_{b,L}}, \end{aligned} \tag{23}$$

the dimensionless governing equations for examining column buckling of thermally affected tapered nanowires with axial material variation are obtained as:

$$\begin{aligned} &\frac{\mathrm{d}}{\mathrm{d}\xi}\left[\chi_4^{T}(\xi)\frac{\mathrm{d}^2\overline{w}^{T}}{\mathrm{d}\xi^2}\right] - \frac{\mathrm{d}}{\mathrm{d}\xi}\left[\left(\eta(\xi)+\chi_5^{T}(\xi)\right)\frac{\mathrm{d}\overline{\theta}_y^{T}}{\mathrm{d}\xi}\right] \\ &\quad - \overline{k}_s(\xi)\overline{G}_b(\xi)\overline{A}_b(\xi)\left(\frac{\mathrm{d}\overline{w}^{T}}{\mathrm{d}\xi} - \overline{\theta}_y^{T}\right) + \overline{K}_r^{T}\,\overline{\theta}_y^{T} = 0, \end{aligned} \tag{24a}$$

$$\begin{aligned} &-\frac{\mathrm{d}}{\mathrm{d}\xi}\left[\overline{k}_s(\xi)\overline{G}_b(\xi)\overline{A}_b(\xi)\left(\frac{\mathrm{d}\overline{w}^{T}}{\mathrm{d}\xi} - \overline{\theta}_y^{T}\right)\right] \\ &\quad - \left(\chi_6^{T}(\xi) + \overline{N}_T^{T} - \overline{N}^{T}\right)\frac{\mathrm{d}^2\overline{w}^{T}}{\mathrm{d}\xi^2} + \overline{K}_t^{T}\,\overline{w}^{T} = 0. \end{aligned} \tag{24b}$$

Seeking for an analytical solution to the critical buckling load according to Eqs. (24a) and (24b) is a very problematic job. To overcome such a difficulty, an efficient numerical scheme is proposed in the next part.

4.2 Thermo-Elastic Buckling Analysis of the TBT-Based Nanowire via RKPM

The deformation fields of the neutral axis of the nanowire modeled based on the TBT are discretized by RKPM in the following form:

$$\overline{w}^{T}(\xi) = \sum_{i=1}^{\mathrm{NP}} \phi_i^{w}(\xi)\overline{w}_i^{T}, \quad \overline{\theta}_y^{T}(\xi) = \sum_{i=1}^{\mathrm{NP}} \phi_i^{\theta_y}(\xi)\overline{\theta}_{y_i}^{T}, \tag{25}$$

where ϕ_i^{w} and $\phi_i^{\theta_y}$ are the RKPM's shape functions, and $\overline{w}_i^{T}$ and $\overline{\theta}_{y_i}^{T}$ are the nodal parameter values. Now, Eqs. (24a) and (24b) in order are pre-multiplied by $\delta\overline{\theta}_y^{T}$, and $\delta\overline{w}^{T}$. After taking successful integration by parts and using Eq. (25), one can arrive at the following set of equations:

$$\left(\begin{bmatrix} [\overline{\mathbf{K}}_b^{T}]^{\theta_y\theta_y} & [\overline{\mathbf{K}}_b^{T}]^{\theta_y w} \\ [\overline{\mathbf{K}}_b^{T}]^{w\theta_y} & [\overline{\mathbf{K}}_b^{T}]^{ww} \end{bmatrix} - \begin{bmatrix} [\overline{\mathbf{K}}_g^{T}]^{\theta_y\theta_y} & [\overline{\mathbf{K}}_g^{T}]^{\theta_y w} \\ [\overline{\mathbf{K}}_g^{T}]^{w\theta_y} & [\overline{\mathbf{K}}_g^{T}]^{ww} \end{bmatrix}\right)\begin{Bmatrix} \overline{\mathbf{\Theta}}_y^{T} \\ \overline{\mathbf{w}}^{T} \end{Bmatrix} = \begin{Bmatrix} \mathbf{0} \\ \mathbf{0} \end{Bmatrix}, \tag{26}$$

where the non-vanishing submatrices and vectors are given by:

$$\left[\overline{\mathbf{K}}_b^T\right]_{ij}^{\theta_y\theta_y} = \int_0^1 \left(\left(\overline{k}_s(\xi)\overline{G}_b(\xi)\overline{A}_b(\xi) + \overline{K}_r^T \right) \phi_i^{\theta_y} \phi_j^{\theta_y} + \left(\eta(\xi) + \chi_5^T(\xi) \right) \frac{\mathrm{d}\phi_i^{\theta_y}}{\mathrm{d}\xi} \frac{\mathrm{d}\phi_j^{\theta_y}}{\mathrm{d}\xi} \right) \mathrm{d}\xi, \tag{27a}$$

$$\left[\overline{\mathbf{K}}_b^T\right]_{ij}^{\theta_y w} = -\int_0^1 \left(\overline{k}_s(\xi)\overline{G}_b(\xi)\overline{A}_b(\xi)\, \phi_i^{\theta_y} \frac{\mathrm{d}\phi_j^{w}}{\mathrm{d}\xi} + \chi_4^T(\xi) \frac{\mathrm{d}\phi_i^{\theta_y}}{\mathrm{d}\xi} \frac{\mathrm{d}^2\phi_j^{w}}{\mathrm{d}\xi^2} \right) \mathrm{d}\xi, \tag{27b}$$

$$\left[\overline{\mathbf{K}}_b^T\right]_{ij}^{w\theta_y} = -\int_0^1 \overline{k}_s(\xi)\overline{G}_b(\xi)\overline{A}_b(\xi)\, \frac{\mathrm{d}\phi_i^{w}}{\mathrm{d}\xi} \phi_j^{\theta_y}\, \mathrm{d}\xi, \tag{27c}$$

$$\left[\overline{\mathbf{K}}_b^T\right]_{ij}^{ww} = \int_0^1 \left(\left(\overline{k}_s(\xi)\overline{G}_b(\xi)\overline{A}_b(\xi) + \chi_6^T(\xi) + \overline{N}_T^T \right) \frac{\mathrm{d}\phi_i^{w}}{\mathrm{d}\xi} \frac{\mathrm{d}\phi_j^{w}}{\mathrm{d}\xi} + \overline{K}_t^T\, \phi_i^{w} \phi_j^{w} \right) \mathrm{d}\xi, \tag{27d}$$

$$\left[\overline{\mathbf{K}}_g^T\right]_{ij}^{ww} = \overline{N}^T \int_0^1 \frac{\mathrm{d}\phi_i^{w}}{\mathrm{d}\xi} \frac{\mathrm{d}\phi_j^{w}}{\mathrm{d}\xi}\, \mathrm{d}\xi, \tag{27e}$$

$$\overline{\Theta}_y^T = <\overline{\theta}_{y_1}^T, \overline{\theta}_{y_2}^T, \ldots, \overline{\theta}_{y_{\mathrm{NP}}}^T>^{\mathrm{T}}, \tag{27f}$$

$$\overline{\mathbf{w}}^T = <\overline{w}_1^T, \overline{w}_2^T, \ldots, \overline{w}_{\mathrm{NP}}^T>^{\mathrm{T}}. \tag{27g}$$

For simply supported nanowires modeled via the TBT, the boundary conditions in the dimensionless form read:

$$\overline{w}^T(0) = \overline{w}^T(1) = 0; \quad \overline{M}_{b_y}^T(0) = \overline{M}_{b_y}^T(1) = 0, \tag{28}$$

where $\overline{M}_{b_y}^T = \frac{M_{b_y}^T}{k_s G_{b,L} A_{b,L} l_b}$. To impose the essential conditions from all those given in Eq. (28), the corrected collocation method (Wagner and Liu 2000) is employed. By solving the resulting set of eigenvalue equations for the dimensionless buckling loads, $\overline{N}_i^T$, the buckling loads of the nanostructure on the basis of the TBT are readily evaluated by: $N_i^T = k_s G_{b,L} A_{b,L}\, \overline{N}_i^T$. The lowest buckling load (i.e., N_{cr}^T) represents the critical buckling load of the thermally affected non-prismatic nanowire with varying material properties.

5 Axially Thermo-Elastic Buckling Based on the Surface Energy-Based HOBT

5.1 Governing Equations Using the HOBT

By employing the HOBT of Reddy and Bickford, the displacement fields of the surface layer as well as those of the bulk as a function of the deformations of the neutral axis of the nanowire are expressed by:

$$\begin{aligned} u_x^H(x,y,z) &= -\left[\left(z - \alpha(x) z^3 \right) \psi_y^H(x) + \alpha(x) z^3 \frac{\mathrm{d}w^H(x)}{\mathrm{d}x} \right], \\ u_z^H(x,y,z) &= w^H(x), \end{aligned} \tag{29}$$

where ψ_y^H is the angle of rotation of the neutral axis about the y-axis, w^H represents the deflection of the neutral axis in the z direction, and $\alpha(x) = \frac{4}{3D_0^2(x)}$ ensures us on the vanishing of the shear stress on the outermost surface of the nanowire.

In the framework of small deformations, the only strains of the bulk are given by:

$$\begin{aligned} \epsilon_{xx}^H &= -\left[\left(z - \alpha(x) z^3 \right) \frac{\mathrm{d}\psi_y^H}{\mathrm{d}x} + \alpha z^3 \frac{\mathrm{d}^2 w^H}{\mathrm{d}x^2} \right], \\ \gamma_{xz}^H &= \left(1 - 3\alpha(x) z^2 \right) \left(\frac{\mathrm{d}w^H}{\mathrm{d}x} - \psi_y^H \right). \end{aligned} \tag{30}$$

Additionally, the stresses within the surface layer are related to the deformation field of the neutral axis by the following relations:

$$\begin{aligned} \tau_{xx}^H &= \tau_0(x) - \left(\lambda_0(x) + 2\mu_0(x) \right) \left[\left(z - \alpha(x) z^3 \right) \frac{\mathrm{d}\psi_y^H}{\mathrm{d}x} + \alpha(x) z^3 \frac{\mathrm{d}^2 w^H}{\mathrm{d}x^2} \right], \\ \tau_{xz}^H &= n_z \tau_0(x) \frac{\mathrm{d}w^H}{\mathrm{d}x}. \end{aligned} \tag{31}$$

For more accurate predicting the mechanical behavior of the nanostructure, it is assumed that the bulk's normal stresses along the z-axis would vary linearly across the diameter between their surface layer's counterparts. Hence,

$$\sigma_{zz}^H = \frac{2z\, \tau_0(x)}{D_0(x)} \frac{\mathrm{d}^2 w^H}{\mathrm{d}x^2}. \tag{32}$$

Using generalized Hooke's law, in view of Eqs. (30) and (32), the most important component of the stresses in the bulk, namely σ_{xx}^H, reads:

$$\sigma_{xx}^H = -E_b(x) \left[\left(z - \alpha(x) z^3 \right) \frac{\mathrm{d}\psi_y^H}{\mathrm{d}x} + \alpha(x) z^3 \frac{\mathrm{d}^2 w^H}{\mathrm{d}x^2} \right] + z \frac{2\nu_b(x)\tau_0(x)}{D_0(x)} \frac{\mathrm{d}^2 w^H}{\mathrm{d}x^2}. \tag{33}$$

Furthermore, based on the given strains in Eq. (30), the only shear stress field in the bulk is provided by:

$$\sigma_{xz}^H = \left(1 - 3\alpha(x) z^2 \right) G_b(x) \left(\frac{\mathrm{d}w^H}{\mathrm{d}x} - \psi_y^H \right). \tag{34}$$

In the context of the HOBT, the strain energy of the thermally affected nanowire with varying cross section accounting for the surface energy effect is given by:

$$U^H = \frac{1}{2}\int_0^{l_b}\left(\begin{array}{l}\frac{\mathrm{d}\psi_y^H}{\mathrm{d}x}M_{b_y}^H + \left(\psi_y^H + \frac{\mathrm{d}w^H}{\mathrm{d}x}\right)\left(\alpha\frac{\mathrm{d}P_{b_y}^H}{\mathrm{d}x} + Q_{b_z}^H\right)\\ +(N_T - N)\left(\frac{\mathrm{d}w^H}{\mathrm{d}x}\right)^2 + K_t\,(w^H)^2 + K_r\left(\psi_y^H\right)^2\end{array}\right)\mathrm{d}x + \frac{1}{2}\int_0^{l_b}\int_{\mathcal{S}}(\tau_{xx}^H\epsilon_{xx}^H + \tau_{xz}^H\gamma_{xz}^H)\mathrm{d}\mathcal{S}\mathrm{d}x, \tag{35a}$$

where the first-order and the third-order moments about the y-axis, namely $M_{b_y}^H$ and $P_{b_y}^H$, as well as the resultant shear force along the z-axis, $Q_{b_z}^H$, are as follows:

$$M_{b_y}^H = \int_{A_b(x)} z\sigma_{xx}^H\,\mathrm{d}A = -\left[(J_2(x) - \alpha(x)J_4(x))\frac{\mathrm{d}\psi_y^H}{\mathrm{d}x} + \alpha(x)J_4(x)\frac{\mathrm{d}^2w^H}{\mathrm{d}x^2}\right] + \frac{2v_b(x)I_2'(x)\tau_0(x)}{D_0(x)}\frac{\mathrm{d}^2w^H}{\mathrm{d}x^2}, \tag{36a}$$

$$P_{b_y}^H = \int_{A_b(x)} z^3\sigma_{xx}^H\,\mathrm{d}A = -\left[(J_4(x) - \alpha(x)J_6(x))\frac{\mathrm{d}\psi_y^H}{\mathrm{d}x} + \alpha(x)J_6(x)\frac{\mathrm{d}^2w^H}{\mathrm{d}x^2}\right] + \frac{2v_b(x)I_4'(x)\tau_0(x)}{D_0(x)}\frac{\mathrm{d}^2w^H}{\mathrm{d}x^2}, \tag{36b}$$

$$Q_{b_z}^H = \kappa(x)\left(\frac{\mathrm{d}w^H}{\mathrm{d}x} - \psi_y^H\right), \tag{36c}$$

and

$$\begin{aligned}\kappa(x) &= \int_{A_b(x)} G_b(x)\left(1 - 3\alpha(x)z^2\right)\mathrm{d}A,\\ I_m'(x) &= \int_{A_b(x)} z^m\,\mathrm{d}A, \quad I_m^{*}(x) = \int_{\mathcal{S}(x)} z^m\,\mathrm{d}\mathcal{S};\ m = 2,4,\\ J_n(x) &= \int_{A_b(x)} E_b(x)\,z^n\,\mathrm{d}A, \quad I_n(x) = \int_{A_b(x)} \rho_b(x)\,z^n\,\mathrm{d}A,\\ I_n^*(x) &= \int_{\mathcal{S}(x)} \rho_0(x)z^n\,\mathrm{d}\mathcal{S}; \quad n = 0,2,4,6.\end{aligned} \tag{37}$$

By exploiting Hamilton's principle, the governing equations associated with column buckling of cross-varying nanowires subjected to axial thermal field via the HOBT are obtained as:

$$-\frac{\mathrm{d}M_{b_y}^H}{\mathrm{d}x} + \alpha\frac{\mathrm{d}P_{b_y}^H}{\mathrm{d}x} + Q_{b_y}^H - \int_{\mathcal{S}} z\frac{\mathrm{d}\tau_{xx}^H}{\mathrm{d}x}\,\mathrm{d}\mathcal{S} + K_r\,\psi_y^H = 0, \tag{38a}$$

$$-\frac{\mathrm{d}Q_{b_z}^H}{\mathrm{d}x} - \alpha\frac{\mathrm{d}^2P_{b_y}^H}{\mathrm{d}x^2} - \int_{\mathcal{S}}\frac{\mathrm{d}\tau_{xz}^H}{\mathrm{d}x}n_z\,\mathrm{d}\mathcal{S} + (N - N_T)\frac{\mathrm{d}^2w^H}{\mathrm{d}x^2} + K_t\,w^H = 0, \tag{38b}$$

by introducing Eqs. (31) and (36a)–(36c), to Eqs. (38a) and (38b), the governing equations of the axially loaded AVNWs under axial thermal gradients on the basis of the HOBT take the following form:

$$\begin{aligned}&\frac{\mathrm{d}}{\mathrm{d}x}\Big[(\alpha(x)J_4(x) - \alpha^2(x)J_6(x) + (\lambda_0(x) + 2\mu_0(x))\alpha(x)I_4'^{*}(x)\\ &\quad - \frac{2v_b(x)\tau_0(x)}{D_0(x)}\left(I_2'(x) - \alpha(x)I_4'(x)\right)\Big)\frac{\mathrm{d}^2w^H}{\mathrm{d}x^2} - (J_2(x)\\ &\quad - 2\alpha(x)J_4(x) + \alpha^2(x)J_6(x) + (\lambda_0(x) + 2\mu_0(x))\big(I_2'^{*}(x)\\ &\quad - \alpha I_4'^{*}(x)\big)\Big)\frac{\mathrm{d}\psi_y^H}{\mathrm{d}x}\Big] - \kappa(x)\left(\frac{\mathrm{d}w^H}{\mathrm{d}x} - \psi_y^H\right) + K_r\,\psi_y^H = 0,\end{aligned} \tag{39a}$$

$$\begin{aligned}&-\frac{\mathrm{d}}{\mathrm{d}x}\left[\kappa(x)\left(\frac{\mathrm{d}w^H}{\mathrm{d}x} - \psi_y^H\right)\right] - \frac{\mathrm{d}}{\mathrm{d}x}\\ &\left[\left(\tau_0(x)S_0^*(x) + N_T - N\right)\frac{\mathrm{d}w^H}{\mathrm{d}x}\right] + \frac{\mathrm{d}^2}{\mathrm{d}x^2}\\ &\Bigg[\left(\alpha(x)J_4(x) - \alpha^2(x)J_6(x)\right)\frac{\mathrm{d}\psi_y^H}{\mathrm{d}x} + \big(\alpha^2(x)J_6(x)\\ &\quad - \frac{2\alpha(x)v_b(x)I_4'(x)\tau_0(x)}{D_0(x)}\big)\frac{\mathrm{d}^2w^H}{\mathrm{d}x^2}\Bigg] + K_tw^H = 0.\end{aligned} \tag{39b}$$

To explore the problem more conveniently, the following dimensionless quantities are taken into account:

$$\begin{aligned}\overline{w}^H &= \frac{w^H}{l_b}, \quad \overline{\psi}_y^H = \psi_y^H, \quad \gamma_1^2(\xi) = \frac{\alpha(x)I_4(x) - \alpha^2(x)I_6(x)}{I_{0,L}l_b^2},\\ \gamma_2^2(\xi) &= \frac{\alpha^2(x)I_6(x)}{I_{0,L}l_b^2}, \quad \gamma_3^2(\xi) = \frac{\kappa(x)l_b^2}{\alpha_L^2J_{6,L}},\\ \gamma_4^2(\xi) &= \frac{\alpha(x)J_4(x) - \alpha^2(x)J_6(x)}{\alpha_L^2J_{6,L}},\\ \gamma_6^2(\xi) &= \frac{\alpha(x)I_4(x) - \alpha^2(x)I_6(x)}{I_{2,L} - 2\alpha_LI_{4,L} + \alpha_L^2I_{6,L}},\\ \gamma_7^2(\xi) &= \frac{\kappa(x)I_{0,L}l_b^4}{(I_{2,L} - 2\alpha_LI_{4,L} + \alpha_L^2I_{6,L})\alpha_L^2J_{6,L}},\\ \gamma_8^2(\xi) &= \frac{(J_2(x) - 2\alpha(x)J_4(x) + \alpha^2(x)J_6(x))I_{0,L}l_b^2}{(I_{2,L} - 2\alpha_LI_{4,L} + \alpha_L^2I_{6,L})\alpha_L^2J_{6,L}},\\ \gamma_9^2(\xi) &= \frac{(\alpha(x)J_4(x) - \alpha^2(x)J_6(x))I_{0,L}l_b^2}{(I_{2,L} - 2\alpha_LI_{4,L} + \alpha_L^2I_{6,L})\alpha_L^2J_{6,L}},\\ \overline{K}_t^H &= \frac{K_tl_b^2}{\alpha_L^2J_{6,L}}, \quad \overline{N}^H = \frac{Nl_b^2}{\alpha_L^2J_{6,L}}, \quad \overline{N}_T^H = \frac{N_Tl_b^2}{\alpha_L^2J_{6,L}},\\ \overline{K}_r^H &= \frac{K_rI_{0,L}l_b^4}{(I_{2,L} - 2\alpha_LI_{4,L} + \alpha_L^2I_{6,L})\alpha_L^2J_{6,L}},\\ \chi_1^H(\xi) &= \frac{I_2^*(x) - 2\alpha I_4^*(x) + \alpha^2I_6^*(x)}{I_{2,L} - 2\alpha_LI_{4,L} + \alpha_L^2I_{6,L}}, \quad \chi_2^H(\xi) =\\ &\quad \frac{\alpha(x)I_4^*(x) - \alpha^2(x)I_6^*(x) - \frac{2v_b(x)\rho_0(x)}{D_0(x)}\left(I_2'(x) - \alpha(x)I_4'(x)\right)}{I_{2,L} - 2\alpha_LI_{4,L} + \alpha_L^2I_{6,L}},\\ \chi_3^H(\xi) &= \frac{\left((\lambda_0(x) + 2\mu_0(x)) - \frac{2v_b(x)\tau_0(x)}{D_0(x)}\left(I_2'(x) - \alpha(x)I_4'(x)\right)\right)I_{0,L}l_b^2}{(I_{2,L} - 2\alpha_LI_{4,L} + \alpha_L^2I_{6,L})\alpha_L^2J_{6,L}},\\ \chi_4^H(\xi) &= \frac{\left((\lambda_0(x) + 2\mu_0(x))\left(I_2^*(x) - \alpha(x)I_4^*(x)\right)\right)I_{0,L}l_b^2}{(I_{2,L} - 2\alpha_LI_{4,L} + \alpha_L^2I_{6,L})\alpha_L^2J_{6,L}},\end{aligned}$$

$$\chi_5^H(\xi)=\frac{\rho_0(x)S_0^*(x)+\frac{2\alpha(x)v_b(x)I_4'(x)\rho_0(x)}{D_0(x)}}{I_{0,L}},$$
$$\chi_6^H(\xi)=\frac{\tau_0(x)S_0^*(x)l_b^2}{\alpha_L^2 J_{6,L}},$$
$$\chi_7^H(\xi)=\frac{2v_b(x)I_4'(x)\tau_0(x)}{\alpha_L J_{6,L}D_0(x)},\ \varrho_1^H(\xi)=\frac{I_2(x)-2\alpha I_4(x)+\alpha^2 I_6(x)}{I_{2,L}-2\alpha_L I_{4,L}+\alpha_L^2 I_{6,L}},$$
$$\varrho_5^H(\xi)=\frac{I_0(x)}{I_{0,L}},\qquad \varrho_7^H(\xi)=\frac{\alpha^2(x)J_6(x)}{\alpha_l^2 J_{6,L}},\tag{40}$$

by introducing Eq. (40) to Eqs. (39a) and (39b), it is obtainable:

$$-\frac{\mathrm{d}}{\mathrm{d}\xi}\left[\left(\gamma_9^2(\xi)+\chi_3^H(\xi)\right)\frac{\mathrm{d}^2\overline{w}^H}{\mathrm{d}\xi^2}+\left(\gamma_8^2(\xi)+\chi_4^H(\xi)\right)\frac{\mathrm{d}\overline{\psi}_y^H}{\mathrm{d}\xi}\right]-\gamma_7^2(\xi)\left(\frac{\mathrm{d}\overline{w}^H}{\mathrm{d}\xi}-\overline{\psi}_y^H\right)+\overline{K}_r^H\,\overline{\psi}_y^H=0,\tag{41a}$$

$$-\frac{\mathrm{d}}{\mathrm{d}\xi}\left[\gamma_3^2(\xi)\left(\frac{\mathrm{d}\overline{w}^H}{\mathrm{d}\xi}-\overline{\psi}_y^H\right)+\left(\chi_6^H(\xi)+\overline{N}_T^H-\overline{N}^H\right)\frac{\mathrm{d}\overline{w}^H}{\mathrm{d}\xi}\right]+\frac{\mathrm{d}^2}{\mathrm{d}\xi^2}\left[\gamma_4^2(\xi)\frac{\mathrm{d}\overline{\psi}_y^H}{\mathrm{d}\xi}\right]+\frac{\mathrm{d}^2}{\mathrm{d}\xi^2}\left[\left(\varrho_7^H(\xi)-\chi_7^H(\xi)\right)\frac{\mathrm{d}^2\overline{w}^H}{\mathrm{d}\xi^2}\right]+\overline{K}_t^H\overline{w}^H=0.\tag{41b}$$

Equations (41a) and (41b) furnish us regarding the governing equations pertinent to the elastic buckling of the thermally affected nanowires with variable cross section and materials across the length based on the HOBT. Finding an analytical solution to these relations is a very cumbersome job. In the following section, an efficient numerical methodology is proposed.

5.2 Thermo-Elastic Buckling Analysis of the HOBT-Based Nanowire via RKPM

The Galerkin–RKPM-based approach is adopted to construct the weak version of Eqs. (41a) and (41b). To this end, the dimensionless deformation fields of the neutral axis are discretized as:

$$\overline{w}^H(\xi)=\sum_{i=1}^{\mathrm{NP}}\phi_i^w(\xi)\overline{w}_i^H,\quad \overline{\psi}_y^H(\xi)=\sum_{i=1}^{\mathrm{NP}}\phi_i^{\psi_y}(\xi)\overline{\psi}_{y_i}^H.\tag{42}$$

Now both sides of Eqs. (41a) and (41b) are pre-multiplied by $\delta\overline{\psi}_y^H$, and $\delta\overline{w}^H$, respectively, and the resulted expressions are integrated over the dimensionless spatial domain of the nanowire. By taking the required integration by parts in view of Eq. (42), the following set of linear equations are obtained:

$$\left(\begin{bmatrix}[\overline{\mathbf{K}}_b^H]^{\psi_y\psi_y} & [\overline{\mathbf{K}}_b^H]^{\psi_y w}\\ [\overline{\mathbf{K}}_b^H]^{w\psi_y} & [\overline{\mathbf{K}}_b^H]^{ww}\end{bmatrix}-\begin{bmatrix}[\overline{\mathbf{K}}_g^H]^{\psi_y\psi_y} & [\overline{\mathbf{K}}_g^H]^{\psi_y w}\\ [\overline{\mathbf{K}}_g^H]^{w\psi_y} & [\overline{\mathbf{K}}_g^H]^{ww}\end{bmatrix}\right)\begin{Bmatrix}\overline{\mathbf{\Psi}}_y^H\\ \overline{\mathbf{w}}^H\end{Bmatrix}=\begin{Bmatrix}\mathbf{0}\\ \mathbf{0}\end{Bmatrix},\tag{43}$$

where the nonzero dimensionless stiffness and geometrical submatrices as well as the dimensionless nodal parameter value vectors are given in the following:

$$\left[\overline{\mathbf{K}}_b^H\right]_{ij}^{\psi_y\psi_y}=\int_0^1\left(\left(\gamma_7^2(\xi)+\overline{K}_r^H\right)\phi_i^{\psi_y}\phi_j^{\psi_y}+\left(\gamma_8^2(\xi)+\chi_4^H(\xi)\right)\frac{\mathrm{d}\phi_i^{\psi_y}}{\mathrm{d}\xi}\frac{\mathrm{d}\phi_j^{\psi_y}}{\mathrm{d}\xi}\right)\mathrm{d}\xi,\tag{44a}$$

$$\left[\overline{\mathbf{K}}_b^H\right]_{ij}^{\psi_y w}=-\int_0^1\left(\gamma_7^2(\xi)\phi_i^{\psi_y}\frac{\mathrm{d}\phi_j^w}{\mathrm{d}\xi}-\left(\gamma_9^2(\xi)+\chi_3^H(\xi)\right)\frac{\mathrm{d}\phi_i^{\psi_y}}{\mathrm{d}\xi}\frac{\mathrm{d}^2\phi_j^w}{\mathrm{d}\xi^2}\right)\mathrm{d}\xi,\tag{44b}$$

$$\left[\overline{\mathbf{K}}_b^H\right]_{ij}^{w\psi_y}=-\int_0^1\left(\gamma_3^2(\xi)\frac{\mathrm{d}\phi_i^w}{\mathrm{d}\xi}\phi_j^{\psi_y}-\gamma_4^2(\xi)\frac{\mathrm{d}^2\phi_i^w}{\mathrm{d}\xi^2}\frac{\mathrm{d}\phi_j^{\psi_y}}{\mathrm{d}\xi}\right)\mathrm{d}\xi,\tag{44c}$$

$$\left[\overline{\mathbf{K}}_b^H\right]_{ij}^{ww}=\int_0^1\begin{pmatrix}\left(\gamma_3^2(\xi)+\chi_6^H(\xi)+\overline{N}_T^H\right)\frac{\mathrm{d}\phi_i^w}{\mathrm{d}\xi}\frac{\mathrm{d}\phi_j^w}{\mathrm{d}\xi}\\ +\left(\varrho_7^H(\xi)-\chi_7^H(\xi)\right)\frac{\mathrm{d}^2\phi_i^w}{\mathrm{d}\xi^2}\frac{\mathrm{d}^2\phi_j^w}{\mathrm{d}\xi^2}+\overline{K}_t^H\phi_i^w\phi_j^w\end{pmatrix}\mathrm{d}\xi,\tag{44d}$$

$$\left[\overline{\mathbf{K}}_g^H\right]_{ij}^{ww}=\overline{N}^H\int_0^1\frac{\mathrm{d}\phi_i^w}{\mathrm{d}\xi}\frac{\mathrm{d}\phi_j^w}{\mathrm{d}\xi}\,\mathrm{d}\xi,\tag{44e}$$

$$\overline{\mathbf{\Psi}}_y^H=<\overline{\psi}_{y_1}^H,\overline{\psi}_{y_2}^H,\ldots,\overline{\psi}_{y_{\mathrm{NP}}}^H>^{\mathrm{T}},\tag{44f}$$

$$\overline{\mathbf{w}}^H=<\overline{w}_1^H,\overline{w}_1^H,\ldots,\overline{w}_{\mathrm{NP}}^H>^{\mathrm{T}}.\tag{44g}$$

For simply supported nanowires modeled on the basis of the HOBT, the following conditions should meet:

$$\overline{w}^H(0)=\overline{w}^H(1)=0;\quad \overline{M}_{b_y}^H(0)=\overline{M}_{b_y}^H(1)=0,\tag{45}$$

where $\overline{M}_{b_y}^H=\frac{M_{b_y}l_b}{\alpha_l^2 J_{6,L}}$. In order to enforce the essential boundary conditions from all those given in Eq. (45), the corrected collocation method (Wagner and Liu 2000) is applied. By solving the resulting set of linear eigenvalue equations for the dimensionless buckling loads, $\overline{N}_{\mathrm{cr},i}^H$ (i.e., $\overline{N}_{\mathrm{cr},1}^H<\overline{N}_{\mathrm{cr},2}^H<\cdots<\overline{N}_{\mathrm{cr},i}^H$), the critical buckling load of the thermally affected AVNW is obtained: $N_{\mathrm{cr}}^H=\frac{\alpha_L^2 J_{6,L}}{l_b^2}\overline{N}_{\mathrm{cr},1}^H$.

6 Results and Discussion

Consider an AVNW in which its materials' properties change longitudinally between those of Al[111] at the left-hand side and those of Si[100] at the right-hand-side. Such properties for these two ends are given by: $E_{b,R} = 210\,\text{GPa}$, $v_{b,R} = 0.24$, $\rho_{b,R} = 2370\,\text{kg/m}^3$, $\mu_{0,R} = -0.6543\,\text{N/m}$, $\lambda_{0,R} = -10\,\text{N/m}$, $\tau_{0,R} = 0.6048\,\text{N/m}$, $\rho_{0,R} = 3.1710^{-7}\,\text{kg/m}^2$, $\alpha_{T,R} = 2.6 \times 10^{-6}/^{\circ}\text{C}$, $k_{t,R} = 280\,\text{W/(m}\,^{\circ}\text{C)}$, $E_{b,L} = 70\,\text{GPa}$, $v_{b,L} = 0.3$, $\rho_{b,L} = 2700\,\text{kg/m}^3$, $\mu_{0,L} = -5.4251\,\text{N/m}$, $\lambda_{0,L} = 3.4939\,\text{N/m}$, $\tau_{0,L} = 0.5689\,\text{N/m}$, $\rho_{0,L} = 5.4610^{-6}\,\text{kg/m}^2$, $\alpha_{T,L} = 23.1 \times 10^{-6}/^{\circ}\text{C}$, and $k_{t,L} = 209\,\text{W/(m}\,^{\circ}\text{C)}$. In the case that the radius of the ends' cross sections has not been explicitly specified, we take the following values: $r_L = 5\,\text{nm}$ and $r_R = 9\,\text{nm}$. The variation of geometry, surface, and bulk properties of the nanowire along its length is assumed as:

$$\begin{aligned} [.](\xi) &= [.]_L + \left([.]_R - [.]_L\right)\xi^{p_g}, \\ \square(\xi) &= \square_L + (\square_R - \square_L)\xi^{p_s}, \\ \diamondsuit(\xi) &= \diamondsuit_L + (\diamondsuit_R - \diamondsuit_L)\xi^{p_m}, \end{aligned} \tag{46}$$

where [.], $\square$, and $\diamondsuit$ represent the properties associated with the geometry, surface layer, and bulk, respectively, p_g, p_s, and p_m in order are their corresponding power-law indices, and parameters with the subscript L or R denote the values of those parameter at the left end or the right end of the nanostructure.

In all carried-out calculations via RKPM, 13 particles with uniform distribution across the length of the nanowire, 6 Gaussian points in each integration cell, and the dilation parameter of value 3.2 times of the interparticle distance have been taken into account. To construct the RKPM's shape functions, the cubic spline window function and the linear base function have been employed.

6.1 Several Comparison Studies

6.1.1 Verification of the Obtained Results by RKPM and Those of the AMM

In the absence of theoretical works on the subject of concern, herein, the predicted results by the RKPM are checked with those of the AMM. In studying the problem using AMM, the unknown fields are expressed in terms of admissible mode shapes that satisfy the geometrical boundary conditions of the nanostructure. For instance, the dimensionless deformation fields of the EBT, TBT, and HOBT for simply supported AVNWs are considered as follows:

$$\begin{aligned} \overline{w}^E(\xi) &= \sum_{i=1}^{\text{NM}} \overline{a}_i^E \sin(i\pi\xi), \\ \overline{w}^T(\xi) &= \sum_{i=1}^{\text{NM}} \overline{a}_i^T \sin(i\pi\xi), \quad \overline{\theta}_y^T(\xi) = \sum_{i=1}^{\text{NM}} \overline{b}_i^T \cos(i\pi\xi), \\ \overline{w}^H(\xi) &= \sum_{i=1}^{\text{NM}} \overline{a}_i^H \sin(i\pi\xi), \quad \overline{\psi}_y^H(\xi) = \sum_{i=1}^{\text{NM}} \overline{b}_i^H \cos(i\pi\xi), \end{aligned} \tag{47}$$

where $\overline{a}_i^E$, $\overline{a}_i^T$, $\overline{b}_i^T$, $\overline{a}_i^H$, and $\overline{b}_i^H$ represent the unknowns pertinent to the ith mode of buckling, NM is the total number of modes (here, NM = 13). The main privilege of the AMM with respect to other numerical methods is that its mode shapes satisfy strong conditions of the problem. Thereby, to evaluate buckling loads based on the Galerkin-AMM, it suffices to substitute these mode shapes into their counterpart shape functions of RKPM in the dimensionless stiffness and geometry stiffness submatrices of the suggested models. Subsequently, by solving the resulted eigenvalue equations for buckling loads, the buckling behavior of the nanostructure could be studied. In Table 1, the predicted first three buckling loads of the simply supported nanostructure by both RKPM and AMM are given in the cases of $p_s = p_m = 2$, $p_g = 1$, $K_t = 0$, and $K_r = 0$. The obtained results are provided for two levels of the temperature gradient (i.e., $\Delta T = 100$ and $200\,^{o}\text{C}$) and four levels of the slenderness ratio (i.e., $\lambda = 10, 20, 40$, and 60). As it is seen, the predicted results by the RKPM based on the EBT, TBT, and HOBT can successfully capture those of the AMM for all considered values of the temperature gradient and slenderness ratio. According to the presented results in Table 1, the discrepancies between the results of various models would reduce by increasing the slenderness ratio. In fact, the effect of shear deformation on the buckling behavior of the nanostructure decreases as the slenderness ratio grows. Additionally, variation of the temperature gradient is more influential on the variation of buckling loads of stockier nanowires. The more detailed roles of temperature gradient and slenderness ratio in the buckling behavior of the nanostructure will be explained in the upcoming parts.

6.1.2 Comparison of the Results of RKPM and Those of Another Work in a Special Case

Consider a macroscale axially functionally graded beam with rectangular cross section whose width(height) varies linearly between $b_L(h_L)$ and $c_b b_L(c_h h_L)$ where b_L and h_L denote the dimensions of the cross section of the beam at the left. The beam under study has simple supports and it is not subjected to any variation of the temperature (i.e., $\overline{N}_T^{[.]} = 0$ where $[.] = E$, T, or H). The variation of the

Table 1 Comparison between the predicted first three buckling loads of the nanostructure by the RKPM and those of the AMM ($p_m = p_m = 2$, $p_g = 1$, $K_l = K_r = 0$)

λ	i	$\Delta T = 100°C$						$\Delta T = 200°C$					
		EBT		TBT		HOBT		EBT		TBT		HOBT	
		RKPM	AMM	RKPM	AMM	RKPM	AMM	RKPM	AMM	RKPM	AMM	RKPM	AMM
10	1	2104.709	2089.365	1183.141	1304.629	1078.012	1197.522	2075.343	2059.999	1153.775	1275.263	1048.646	1168.156
	2	8933.534	8866.202	1925.491	1989.572	1864.936	1886.977	8904.168	8836.836	1896.125	1960.206	1835.569	1857.611
	3	20442.086	20191.609	2281.461	2439.227	2439.431	2462.788	20412.720	20162.243	2252.095	2409.861	2410.064	2433.422
20	1	512.735	508.899	429.358	447.216	414.027	434.198	483.368	479.533	399.991	417.850	384.660	404.832
	2	2220.049	2203.214	1261.024	1263.909	1145.842	1327.851	2190.683	2173.848	1231.658	1234.542	1116.476	1298.485
	3	5097.247	5034.603	1779.733	1821.575	1603.609	1729.006	5067.881	5005.236	1750.366	1792.209	1574.243	1699.640
40	1	114.737	113.779	108.244	109.625	107.090	108.652	85.371	84.412	78.877	80.259	77.724	79.286
	2	541.679	537.469	456.628	456.612	440.648	832.234	512.313	508.103	427.262	427.245	411.282	802.868
	3	1261.038	1245.352	891.402	890.538	833.141	1212.935	1231.672	1215.986	862.035	861.171	803.775	1183.569
60	1	41.027	40.602	39.485	39.757	39.269	39.553	11.661	11.235	10.119	10.390	9.903	10.187
	2	230.873	229.000	211.945	211.817	208.274	446.408	201.507	199.634	182.579	182.451	178.908	417.042
	3	550.630	543.640	464.065	462.761	447.841	1016.448	521.264	514.274	434.699	433.395	418.475	987.082

Young's modulus and the density across the length is assumed to be $E_b(\xi) = E_{b,L}(1+\xi)$ and $\rho_b(\xi) = \rho_{b,L}\left(1+\xi+\xi^2\right)$. For various values of c_b and c_h, the predicted dimensionless axial buckling loads by the suggested models and those of Shahba and Rajasekaran (2012) using differential quadrature element method of lowest order (DQEL) are provided in Table 2. As it is seen, there exists a reasonably good agreement between the predicted results by RKPM and those of Shahba and Rajasekaran (2012) in most of the cases.

6.2 Parametric Studies

In the following subsections, we schedule a fairly comprehensive parametric study to reveal the influences of the influential factors on the thermo-elastic buckling behavior of AVNWs.

6.2.1 The Influence of the Slenderness Ratio

In Fig. 2a–c, the predicted critical buckling load of the nanowire as a function of the slenderness ratio is plotted for three levels of the temperature gradient (i.e., $\Delta T = 100, 500$, and $900\,°C$). The nanowire is free from the surrounding elastic medium, $p_m = p_s = 3$ and $p_g = 2$. Throughout this article, the plotted results based on the CET and the SET are demonstrated by the dashed lines and the solid lines, respectively. Additionally, the results of the EBT, TBT, and HOBT in order are specified by the lines with square, circle, and triangle markers. Irrespective of the considered model, the critical buckling load of the nanowire would reduce as the slenderness ratio increases. The main reason of this fact is the reduction of the transverse stiffness by increasing the nanowire's length. The rate of reduction is more obvious for the plots pertinent to the EBT and the nanowires with lower levels of the slenderness ratio. Commonly, the plotted results based on the TBT are closer to those of the HOBT since both of these theories take into account shear deformation effect in their formulations. The predicted buckling loads by the EBT are usually greater than those of the TBT and the HOBT. It is mainly because of this fact that the EBT has no sense with respect to shear effect; therefore, the factual transverse stiffness is overestimated by the EBT. All the proposed models predict that the buckling load of the nanowire would reduce as the temperature gradient increases. The more accurate influence of the temperature gradient on the buckling behavior of the nanostructure will be explained in the following subsection. In the cases of $\Delta T = 500$ and $900\,°C$, the zero buckling loads are detectable at special levels of the slenderness ratio. The slenderness ratio associated with the zero buckling load is called *critical*

Table 2 Verification of the dimensionless critical buckling loads (i.e., $\overline{N}^{*}_{\mathrm{cr}} = \frac{N^{[.]}_{\mathrm{cr}} l_b^2}{E_{b,L} I_{b,L}}$) based on the suggested models via RKPM and those of Shahba and Rajasekaran (2012)

c_h	Method	c_b				
		0	0.2	0.4	0.6	0.8
0	EBT	14.6195	13.2378	11.7842	10.2206	8.4577
	TBT	14.5076	13.1369	11.6944	10.1424	8.3913
	HOBT	14.5274	13.1548	11.7104	10.1563	8.4032
	Shahba and Rajasekaran (2012)	14.5112	13.1398	11.6969	10.1451	8.3957
0.2	EBT	10.7658	9.6687	8.5173	7.2821	5.8929
	TBT	10.6905	9.6013	8.4580	7.2313	5.8509
	HOBT	10.7039	9.6133	8.4685	7.2403	5.8584
	Shahba and Rajasekaran (2012)	10.6860	9.5971	8.4543	7.2284	5.8498
0.4	EBT	7.3372	6.5195	5.6644	4.7511	3.7289
	TBT	7.2926	6.4801	5.6303	4.7226	3.7064
	HOBT	7.3006	6.4871	5.6364	4.7277	3.7104
	Shahba and Rajasekaran (2012)	7.2831	6.4715	5.6228	4.7164	3.7019
0.6	EBT	4.3604	3.8169	3.2519	2.6529	1.9891
	TBT	4.3413	3.8005	3.2382	2.6422	1.9817
	HOBT	4.3449	3.8035	3.2408	2.6443	1.9831
	Shahba and Rajasekaran (2012)	4.3287	3.7892	3.2283	2.6338	1.9748
0.8	EBT	1.8804	1.6068	1.3255	1.0318	.7131
	TBT	1.8844	1.6109	1.3298	1.0363	.7186
	HOBT	1.8844	1.6109	1.3296	1.0361	.7182
	Shahba and Rajasekaran (2012)	1.8667	1.5950	1.3157	1.0239	.7075

slenderness ratio. In fact for these levels of the slenderness ratio and the given temperature gradient, the nanowire could not bear any axial load and buckles by exertion a small axial force. Among the suggested models, the HOBT(EBT) has the lowest(highest) critical slenderness ratio.

In the case of $\Delta T = 100$, the relative discrepancies between the predicted results by the proposed models would generally decrease by an increase in the slenderness ratio. For $\lambda = 10$, 20, and 30, the EBT(TBT) overestimates the results of the HOBT with relative errors of about 53.8 (7), 14.3 (2.25), and 7.24 (1.1), respectively. For each model, the relative discrepancies between the results of the SET and those of the CET would reduce by increasing the slenderness ratio. The maximum discrepancies are observed for the TBT. In the cases of $\Delta T = 500$ and 900 °C, the relative discrepancies between the predicted results by the EBT or the TBT and those of the HOBT would commonly increase by increasing the slenderness ratio, and the maximum discrepancies are observed at the critical slenderness ratios. For these cases, the role of the surface energy on the buckling behavior of the nanowire becomes highlighted as the slenderness ratio increases. At the critical slenderness ratios, the maximum surface energy effect is detectable for all suggested models.

6.2.2 The Influence of the Temperature Gradient

The plots of the critical buckling load of the thermally affected AVNW in terms of the temperature gradient are provided in Fig. 3a–c for three levels of the slenderness ratio (i.e., $\lambda = 10, 20,$ and 40). The demonstrated results are related to the case of $p_m = p_s = 3$, $p_g = 2$ when the nanowire is released from its surrounding environment. As a general result, the critical buckling load of the nanostructure would reduce by increasing the temperature gradient. Such a reduction is more obvious for higher slender nanowires. A close survey of the plotted results reveals that the relative discrepancies between the proposed models would slowly increase by an increase in the temperature gradient. In the case of $\lambda = 10$ and for $\Delta T = 0, 50,$ and 100 °C, the EBT(TBT) overestimates the results of the HOBT about 51.9 (6.7), 52.8 (6.8), and 53.8 (6.9)%, respectively. In the cases of $\lambda = 10$ and 20, the proposed models based on the CET overestimate the results of the models based on the SET. Additionally, variation of the temperature gradient has a small influence on the variation of the relative discrepancies between the predicted results by the CET's models and those of the SET's ones. However, in the case of $\lambda = 40$, the predicted results by the CET's models underestimate the predicted results by the SET's models for the considered range of the temperature gradient. In such a case, the influence of the surface energy

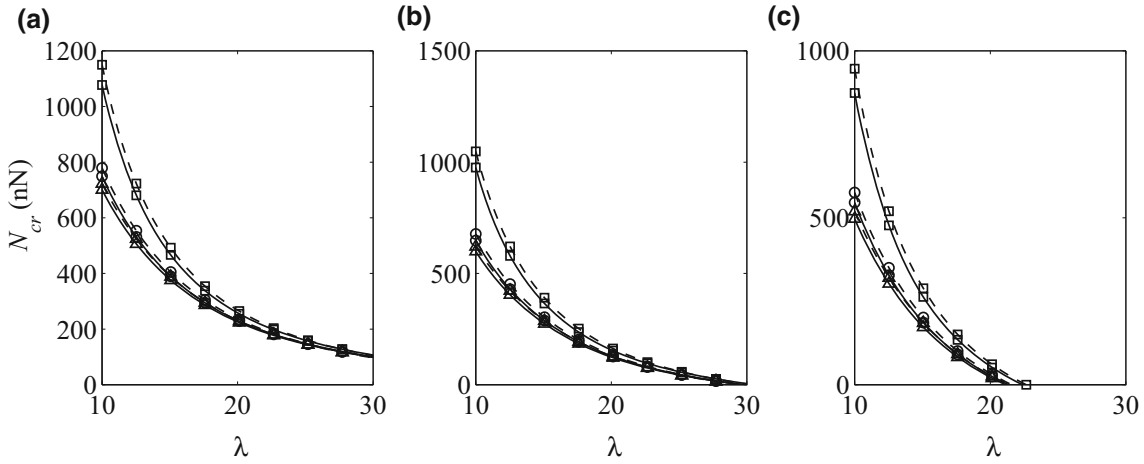

Fig. 2 Critical buckling load of the AVNW as a function of the slenderness ratio for three values of the temperature gradients: **a** $\Delta T = 100$, **b** $\Delta T = 500$, **c** $\Delta T = 900\,^{\circ}\mathrm{C}$; ($p_m = p_s = 3$, $p_g = 2$, $K_t = K_r = 0$; (− − −) SET, (—) CET; (□) EBT, (○) TBT, (△) HOBT)

on the buckling behavior of the nanostructure increases as the temperature gradient increases.

6.2.3 The Influence of the Power-law Index of Material

An important parametric study is conducted to answer this critical question that how variation of the material properties across the nanowire's length could influence on its axial buckling behavior. The predicted critical buckling loads of the AVNW as a function of the power-law index of material are presented in Fig. 4a–c for three levels of the slenderness ratio (i.e., $\lambda = 10, 20$, and 40). The results are presented for AVNWs with $p_g = 2$, $K_t = K_r = 0$, which is subjected to $\Delta T = 200\,^{\circ}\mathrm{C}$. Irrespective of the slenderness ratio, the critical buckling load of the nanostructure decreases as the power-law index of material magnifies. Such a decreasing is more apparent in the case of $\lambda = 40$. As it is seen in these figures, the predicted results by the TBT are generally close to those of the HOBT. In the cases of $\lambda = 10$ and 20, the relative discrepancies between the predicted buckling loads by the EBT and those of the HOBT would increase with the power-law index of material up to a certain level. For the power-law index lower than this particular value, the aforementioned discrepancies would mildly decrease as the power-law index of material grows. For $\lambda = 40$, the relative discrepancies between the predicted buckling loads of various models would obviously magnify as the power-law index of material increases. A close scrutiny of the plotted results shows that the influence of the surface energy on the critical buckling load of the nanowire becomes important by increasing the power-law index of the material. Commonly, such a fact is not affected by the slenderness ratio of the nanowire; however, variation of the power-law index of material is more influential on the variation of the buckling load of more slender nanowires. For example, the HOBT based on the CET could capture the results of the HOBT based on the SET for the set of the material power-law index (0,2.5,5) with relative error about (1.9, 3.1, 3.6), (1.8, 2.6, 2.7), and (2.7, 19.3, 33.8) for the slenderness ratios $\lambda = 10$, 20, and 40, respectively. Additionally, the relative discrepancies between the results of the EBT/TBT/HOBT based on the CET and their corresponding SET-based models are lower than 5% for the power-law index of material lower than (5, 5, 0.58)/(0.8, 5, 0.7)/(5, 5, 0.54) for the set of slenderness ratios $\lambda = (10, 20, 40)$.

6.2.4 The Influence of the Power-law Index of Geometry

To study the role of variation of the nanowire's cross section across the length on its buckling behavior, an investigation is performed. For this purpose, the plots of the buckling load as a function of the power-law index of geometry are presented in Fig. 5a–c for three levels of the slenderness ratio (i.e., $\lambda = 10, 20$, and 40). These results are given for $p_m = p_s = 3$, $K_t = K_r = 0$, and $\Delta T = 200\,^{\circ}\mathrm{C}$. As it is obvious in Fig. 5a–c, the predicted critical buckling load of the nanostructure would usually decrease as the power-law index of geometry increases. For the considered temperature gradient, the obtained graphs consist of two apparent branches: a descending part and a fairly constant part. In the descending branch, the predicted buckling load would harshly decrease with the power-law index of geometry. However, in the fairly constant branch, variation of the power-law index of geometry has moderately no influence on the variation of the critical buckling load of the AVNW. A detailed investigation of the demonstrated results indicates that the relative discrepancies between the predicted results by the EBT or the TBT and those of the HOBT would magnify with the power-law index up to a

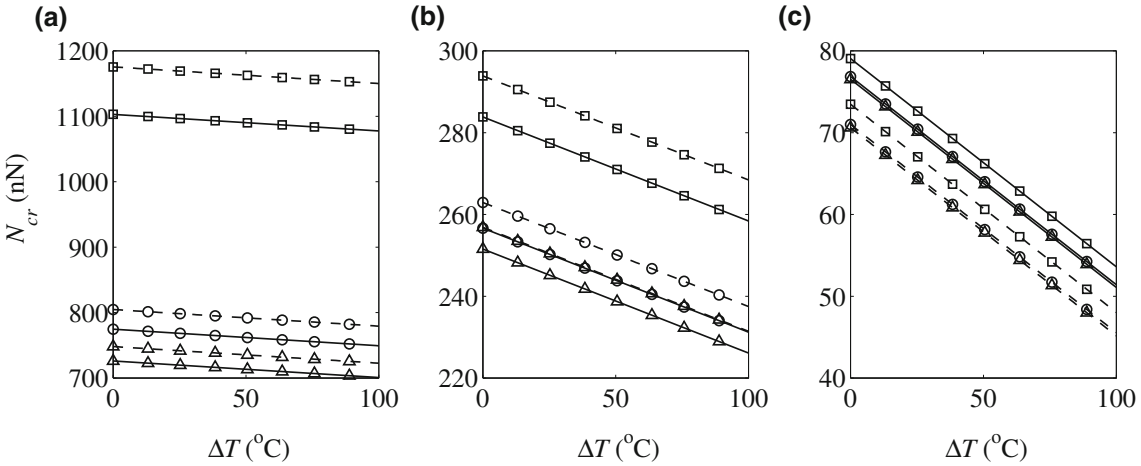

Fig. 3 Critical buckling load of the AVNW as a function of the temperature gradients: **a** $\lambda = 10$, **b** $\lambda = 20$, **c** $\lambda = 40$; ($p_m = p_s = 3$, $p_g = 2$, $K_t = K_r = 0$; (− − −) SET, (—) CET; (□) EBT, (○) TBT, (△) HOBT)

particular value. For power-law indices of geometry greater than this, such relative discrepancies would reduce slowly as the power-law index of geometry increases. For $\lambda = 10, 20$, and 40 and in the context of the SET, the maximum discrepancies between the buckling load by the EBT and those of the HOBT are observed at $p_g \approx 0.3, 0.3$, and 0.4, respectively. In the cases of $\lambda = 10, 20$, and 40, the TBT in order overestimates the predicted results by the HOBT with relative error lower than 12, 6, and 2%. Nevertheless, for these cases, the EBT captures the results of the HOBT with relative error greater than 41, 12, and 6% for the considered range of the power-law index of geometry. For the set of slenderness ratios $\lambda = (10, 20)$, the EBT/TBT/HOBT based on the CET overestimates the results of their counterpart surface elasticity-based models with relative errors lower than (4.1, 3.2)/(6.5, 4.6)/(3.5, 2.8)% for all considered values of the power-law index of geometry. However, in the case of $\lambda = 40$, the relative discrepancies between the predicted buckling load by the models based on the CET and those of the SET would commonly grow as the power-law index of geometry increases. For instance, for $p_g = (0, 2.5, 5)$, the classical models based on the EBT/TBT/HOBT could capture the results of the models on the basis of the SET with relative error about (0.76, 17.17, 24.76)/(0.26, 19.14, 26.74)/(0.12, 19.52, 27.06)%, respectively.

6.2.5 The Influence of the Nanowire's Diameter

We are also interested in this fact that how variation of the nanowire's diameter could influence on the critical buckling load. Additionally, the roles of the surface energy effect as well as the shear deformation on the predicted results for various nanowire's diameters are of concern. To this end, the predicted critical buckling load of the AVNW as a function of the diameter of the left end is plotted in

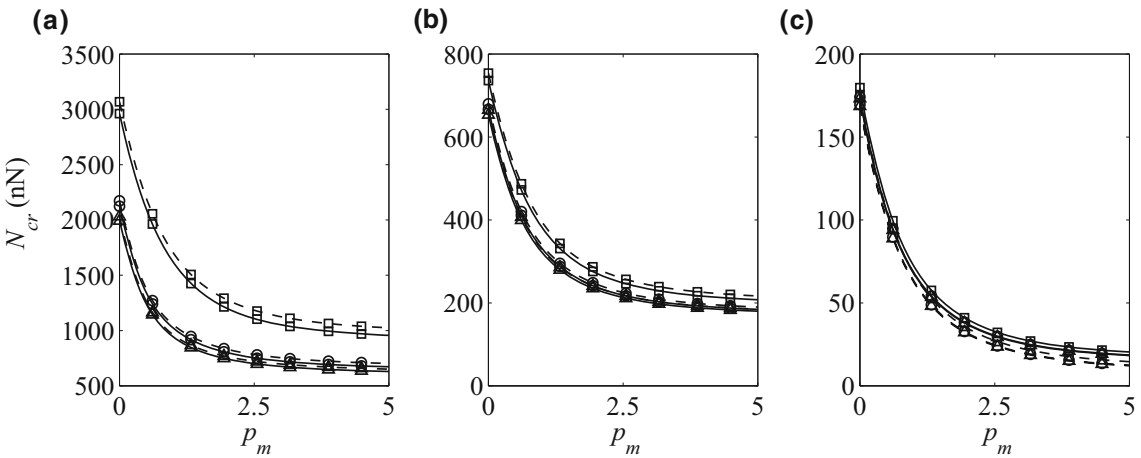

Fig. 4 Critical buckling load of the AVNW as a function of the power-law index of the material property: **a** $\lambda = 10$, **b** $\lambda = 20$, **c** $\lambda = 40$; ($\Delta T = 200\,^{\circ}$C, $p_g = 2$, $K_t = K_r = 0$; (− − −) SET, (—) CET; (□) EBT, (○) TBT, (△) HOBT)

Fig. 6a–c for three levels of the temperature gradients (i.e., $\Delta T = 100, 300$, and 500°C). The demonstrated results have been provided for a freely deformed nanowire (i.e., $K_t = K_r = 0$) of length 40 nm whose geometry and material varies across its length such that $p_m = p_s = 3$ and $p_g = 2$. As it is seen in these figures, the critical buckling load of the nanowire commonly magnify by increasing the left end's diameter. For lower levels of the temperature gradient, variation of the diameter is more influential on the variation of the buckling load. Such a fact is predicted by all suggested models. In the case of $\Delta T = 100\,°\text{C}$, the relative discrepancies between the predicted buckling loads by the EBT and those of the HOBT would generally increase by an increase in the nanowire's diameter. For example, the EBT(TBT) overestimates the results of the HOBT with relative error about 3.9 (0.8), 8.8 (1.4), and 15.3 (2.4)% in the cases of $D_L = 4, 6$, and 8 nm, respectively. In the case of $\Delta T = 300\,°\text{C}$, the relative discrepancies between the results of the EBT or TBT and those of the HOBT would decrease up to a certain nanowire's diameter. For diameters greater than this special one, the relative discrepancies between the results of the EBT or the TBT and those predicted by the HOBT would slightly magnify with the nanowire's diameter. For $D_L = 4, 6$, and 8 nm, the relative discrepancies between the EBT(TBT) results and those of the HOBT in order are about 62.1(12.9), 15.3(2.4), and 20.2(3.2)%. In the case of $\Delta T = 500\,°\text{C}$, the critical buckling load of the nanowire would reduce by reduction of the diameter such that becomes zero at particular values of the nanowire's diameters. This is called *critical diameter of the nanowire*. A close exploration of the obtained results reveals that the relative discrepancies between the obtained results by various models reach to their maximum levels at the critical nanowire's diameter. Generally, the relative discrepancies between the predicted results based on the SET and those of the CET would harshly decrease by increasing the nanowire's diameter up to a particular value. For diameters greater than this special value, the above-mentioned discrepancies would slightly increase as the diameter increases.

6.2.6 The Influence of the Transverse Stiffness of the Matrix

When an AVNW is embedded in a matrix, the transverse stiffness of the surrounding medium could affect on the buckling behavior of the nanostructure. To examine such a fact, the plots of the critical buckling load of the nanowire as a function of the dimensionless transverse stiffness of the matrix for three levels of the slenderness ratio (i.e., $\lambda = 5, 10$, and 30) are demonstrated in Fig. 7a–c. The plotted results are given for thermally affected nanowires with $p_m = p_s = 3$, $p_g = 2$, $K_r = 0$, and $\Delta T = 200\,°\text{C}$. In order to neutralize the effect of the slenderness ratio on the transverse stiffness of the matrix, its dimensionless value is defined by: $\overline{K}_t^* = \overline{K}_t^E \left(\frac{\lambda^*}{\lambda}\right)^4$ where $\lambda^* = 30$. All the proposed models predict that the critical buckling load of the nanostructure would increase by increasing the transverse stiffness of the matrix and the rate of increase is more obvious in more slender nanowires. In very stocky nanowires (i.e., $\lambda \leq 10$), the relative discrepancies between the results of various models are slightly affected by the variation of the transverse stiffness of the matrix. Irrespective of the transverse stiffness of the surrounding medium, the EBT(TBT) commonly overestimates the predicted results by the HOBT with relative error of about 225 (11.8) and 58 (7.5)% for the cases of $\lambda = 5$ and 10, respectively. It also implies that the predicted results by the EBT are not trustable at all for such nanowires. In the case of $\lambda = 30$, the relative discrepancies between the predicted

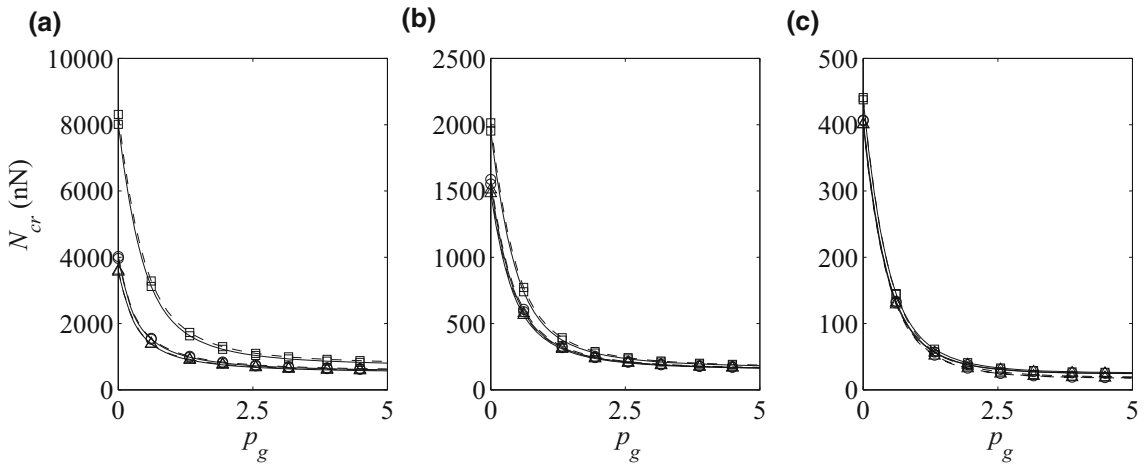

Fig. 5 Critical buckling load of the AVNW as a function of the power-law index of the geometry property: **a** $\lambda = 10$, **b** $\lambda = 20$, **c** $\lambda = 40$; ($\Delta T = 200\,°\text{C}$, $p_m = p_s = 3$, $K_t = K_r = 0$; (− − −) SET, (—) CET; (□) EBT, (○) TBT, (△) HOBT)

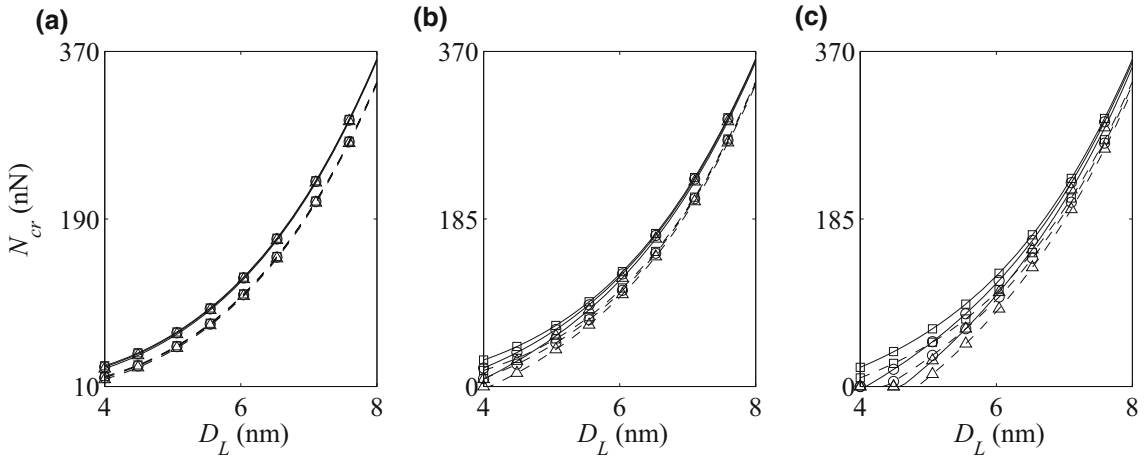

Fig. 6 Critical buckling load of the AVNW as a function of the diameter for three levels of the temperature gradients: **a** $\Delta T = 100$, **b** $\Delta T = 300$, **c** $\Delta T = 500\,^{\circ}\mathrm{C}$; ($l_b = 40\,\mathrm{nm}$, $p_m = p_s = 3$, $p_g = 2$, $K_t = K_r = 0$; (− − −) SET, (—) CET; (□) EBT, (○) TBT, (△) HOBT)

buckling loads by the EBT or TBT and those of the HOBT would decrease by increasing the matrix transverse stiffness up to a particular value. For the transverse stiffness of the matrix greater than this value, such discrepancies would grow as the transverse stiffness of the matrix increases. For $\overline{K}_t^* = 0$, 250, and 500, the EBT (TBT) could reproduce the predicted results by the HOBT with relative error about 14.8 (2.2), 5.7 (0.94), and 7.4 (1.4)%, respectively. Regarding the role of the surface energy on the buckling behavior of the nanostructure, in the case of $\lambda = 5$, surface effect is fairly not affected by the variation of the transverse stiffness of the surrounding medium. In the cases of $\lambda = 10$ and 30, the effect of the surface energy on the predicted results would diminish by increasing the transverse stiffness of the matrix.

6.2.7 The Influence of the Rotational stiffness of the Matrix

We are also interested in the role of rotational stiffness of the surrounding medium on the buckling behavior of the thermally affected AVNW. For this purpose, the plots of the critical buckling load of the nanostructure in terms of the dimensionless rotational stiffness of the matrix are demonstrated in Fig. 8a–c. The presented results are provided for three levels of the slenderness ratio (i.e., $\lambda = 5, 10$, and 30) of the thermally affected nanowire with $p_m = p_s = 3$, $p_g = 2$, $K_t = 0$, and $\Delta T = 200\,^{\circ}\mathrm{C}$. Let define the dimensionless rotational stiffness of the matrix as follows: $\overline{K}_r^* = \overline{K}_r^E \left(\frac{\lambda^*}{\lambda}\right)^2$ where $\lambda^* = 30$. According to the plotted results in Fig. 8a–c, irrespective of the slenderness ratio of the nanowire, the critical buckling load would magnify as the rotational stiffness of the surrounding medium increases. Such an issue is more obvious for more slender nanowires (see Fig. 8c). In fact, variation of the rotational stiffness of the matrix is more influential on buckling load of AVNWs with higher slenderness ratios. The plots associated with the TBT are commonly closer to those of the HOBT since the shear deformation effect is taken into account by these models. A close survey of the plotted results shows that the relative discrepancies between the predicted buckling loads by the EBT or the TBT and those of the HOBT would generally increase by an increase in the rotational stiffness of the matrix. In the cases of $\lambda = 10$ and 30, the EBT overestimates the predicted results by the HOBT with relative error about (58, 78.1, 98.5) and (14.8, 32.5, 54.6) for $\overline{K}_r^* = (0, 50, 100)$, respectively. For similar cases, the TBT in order captures the results of the HOBT with relative error about (7.5, 12.3, 16.4) and (2.2, 10.6, 17.4). Concerning the role of the surface energy on the predicted critical buckling loads, a detailed scrutiny of the plotted results indicates that relative discrepancies between the obtained results based on the SET and those of the CET would generally decrease by increasing the rotational stiffness of the matrix. Such a reduction is also more apparent for more slender nanowires. In other words, the influence of the surface energy on the buckling behavior of the nanowire would reduce as the rotational stiffness grows. For example, in the case of $\lambda = 30$, the HOBT based on the SET overestimates the results of the CET with relative error about 5.3, 1.5, and 1.1% for $\overline{K}_r^* = 0, 50$, and 100, respectively.

7 Conclusions

Axial buckling behavior of thermally affected AVNW was investigated in the context of the surface elasticity theory of Gurtin–Murdoch. To this end, the governing equations were constructed based on the EBT, TBT, and HOBT. Due to non-uniformity of the nanowire's cross section as well as

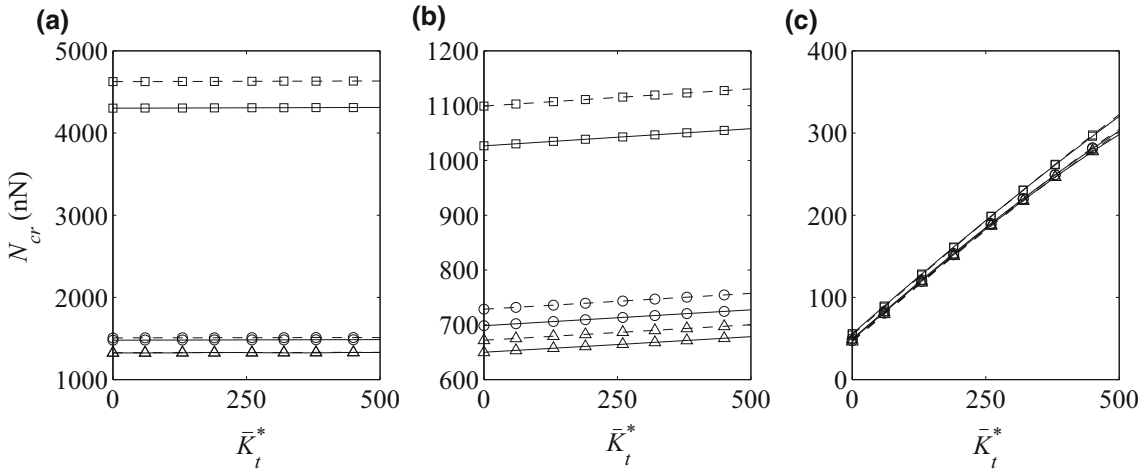

Fig. 7 Critical buckling load of the AVNW as a function of the transverse stiffness of the surrounding medium: **a** $\lambda = 5$, **b** $\lambda = 10$, **c** $\lambda = 30$; ($\Delta T = 200\,^{\circ}\mathrm{C}$, $p_g = 2$, $p_m = p_s = 3$, $K_r = 0$; (− − −) SET, (—) CET; (□) EBT, (○) TBT, (△) HOBT)

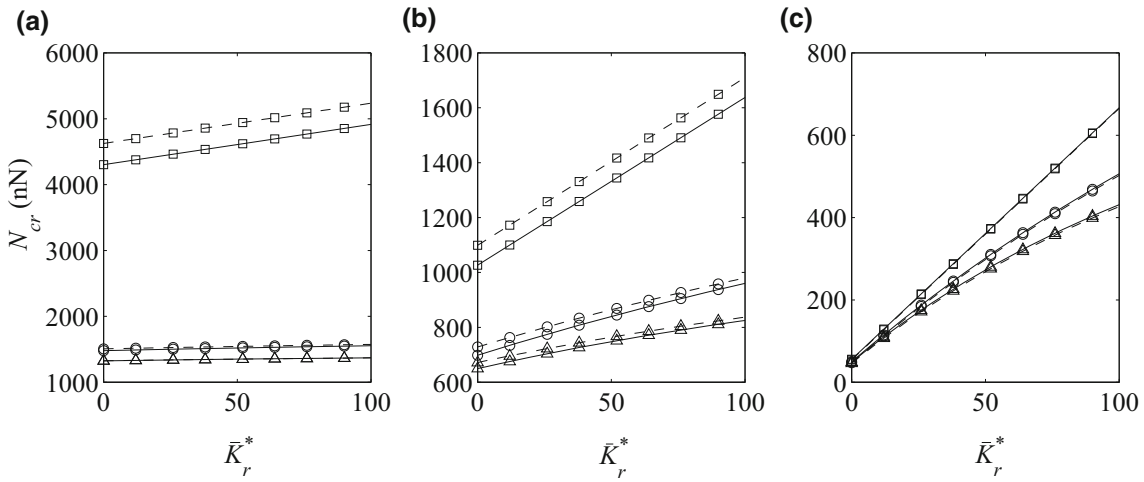

Fig. 8 Critical buckling load of the AVNW as a function of the rotational stiffness of the surrounding medium: **a** $\lambda = 5$, **b** $\lambda = 10$, **c** $\lambda = 30$; ($\Delta T = 200\,^{\circ}\mathrm{C}$, $p_g = 2$, $p_m = p_s = 3$, $K_t = 0$; (− − −) SET, (—) CET; (□) EBT, (○) TBT, (△) HOBT)

variation of the material property along the nanowire, finding an analytical solution to the governing equations is a cumbersome task. As an alternative methodology, RKPM was proposed and the critical buckling loads of the nanowire were calculated. In a special case, the predicted results by the RKPM were compared with those of AMM and a reasonably good agreement was obtained. Subsequently, the roles of the slenderness ratio, nanowire's diameter, power-law indices of geometry and material, temperature gradient, transverse and rotational stiffness of the surrounding medium on the critical buckling load of the nanostructure were addressed in some detail. Additionally, the roles of shear deformation and surface effects on the obtained results were discussed and explained.

Commonly, the surface elasticity-based-beam models are appropriately affected by the diameter of nanowires, while the nonlocal continuum-based ones are more sensitive with respect to the nanowire's length. To employ the privileges of these two ones in modeling of the buckling and postbuckling of AVNWs, a suitable combination of the nonlocal- and surface elasticity-based theories would be a wise decision. Further, the present work could be regarded as a basic bed for more advanced researches on thermoelastic buckling and vibration of vertically aligned tapered nanowires with arbitrary distribution of material across the length. Owing to high potential applications of ensembles of nanowires in NEMS, these crucial issues should be followed up seriously by the applied mechanics and other related communities.

References

Ahn K, Kim K, Kim J (2015) Thermal conductivity and electric properties of epoxy composites filled with TiO_2-coated copper nanowire. Polymer 76:313–320

Ansari R, Gholami R, Darabi MA (2011) Thermal buckling analysis of embedded single-walled carbon nanotubes with arbitrary boundary conditions using the nonlocal Timoshenko beam theory. J Thermal Stresses 34:1271–1281

Ansari R, Mohammadi V, Shojaei MF, Gholami R, Sahmani S (2013) Postbuckling characteristics of nanobeams based on the surface elasticity theory. Compos Part B Eng 55:240–246

Barth JV, Costantini G, Kern K (2005) Engineering atomic and molecular nanostructures at surfaces. Nature 437:671–679

Chen JS, Pan C, Wu CT, Liu WK (1996) Reproducing kernel particle methods for large deformation analysis of non-linear structures. Comput Methods Appl Mech Eng 139:195–227

Chen R, Lu MC, Srinivasan V, Wang Z, Cho HH, Majumdar A (2009) Nanowires for enhanced boiling heat transfer. Nano Lett 9:548–553

Cheng F, Liang J, Tao Z, Chen J (2011) Functional materials for rechargeable batteries. Adv Mater 23:1695–1715

Chiu MS, Chen T (2012) Effects of high-order surface stress on buckling and resonance behavior of nanowires. Acta Mech 223:1473–1484

Cuenot S, Fretigny C, Demoustier-Champagne S, Nysten B (2004) Surface tension effect on the mechanical properties of nanomaterials measured by atomic force microscopy. Phys Rev B 69:165410

Duarte EA, Quintero PA, Meisel MW, Nino JC (2013) Electrospinning synthesis of superconducting BSCCO nanowires. Physica C 495:109–113

Eltaher MA, Emam SA, Mahmoud FF (2013) Static and stability analysis of nonlocal functionally graded nanobeams. Compos Struct 96:82–88

Farajpour A, Dehghany M, Shahidi AR (2013) Surface and nonlocal effects on the axisymmetric buckling of circular graphene sheets in thermal environment. Compos Part B Eng 50:333–343

Gordon MJ, Baron T, Dhalluin F, Gentile P, Ferret P (2009) Size effects in mechanical deformation and fracture of cantilevered silicon nanowires. Nano Lett 9:525–529

Gurtin ME, Murdoch AI (1975) A continuum theory of elastic material surfaces. Arch Ration Mech Anal 57:291–323

Gurtin ME, Murdoch AI (1976) Effect of surface stress on wave propagation in solids. J Appl Phys 47:4414–4421

Hasheminejad SM, Gheshlaghi B, Mirzaei Y, Abbasion S (2011) Free transverse vibrations of cracked nanobeams with surface effects. Thin Solid Films 519:2477–2482

Hochbaum AI, Fan R, He R, Yang P (2005) Controlled growth of Si nanowire arrays for device integration. Nano Lett 5:457–460

Hu KM, Zhang WM, Zhong ZY, Peng ZK, Meng G (2014) Effect of surface layer thickness on buckling and vibration of nonlocal nanowires. Phys Lett A 378:650–654

Jing GY, Duan HL, Sun XM, Zhang ZS, Xu J, Li YD, Wang JX, Yu DP (2006) Surface effects on elastic properties of silver nanowires: contact atomic-force microscopy. Phys Rev B 73:235409

Jun S, Liu WK, Belytschko T (1998) Explicit reproducing kernel particle methods for large deformation problems. Int J Numer Methods Eng 41:137–166

Juntarasaid C, Pulngern T, Chucheepsakul S (2012) Bending and buckling of nanowires including the effects of surface stress and nonlocal elasticity. Physica E 46:68–76

Kiani K (2015) Column buckling of magnetically affected stocky nanowires carrying electric current. J Phys Chem Solids 83:140–151

Kiani K (2015) Axial buckling analysis of a slender current-carrying nanowire acted upon by a magnetic field using the surface energy approach. J Phys D Appl Phys 48:245302

Kiani K (2016a) Thermo-elasto-dynamic analysis of axially functionally graded non-uniform nanobeams with surface energy. Int J Eng Sci 106:57–76

Kiani K (2016b) Column buckling of doubly parallel slender nanowires carrying electric current acted upon by a magnetic field. J Phys Chem Solids 95:89–97

Kiani K (2016c) Elastic buckling of current-carrying double-nanowire-systems immersed in a magnetic field. Acta Mech 227(12):3549–3570

Kiani K (2017a) Exact postbuckling analysis of highly stretchable-surface energetic-elastic nanowires with various ends conditions. Int J Mech Sci 124:242–252

Kiani K (2017b) Postbuckling scrutiny of highly deformable nanobeams: a novel exact nonlocal-surface energy-based model. J Phys Chem Solids 110:327–343

Korneev A, Korneeva Y, Florya I, Voronov B, Goltsman G (2012) NbN nanowire superconducting single-photon detector for mid-infrared. Phys Proc 36:72–76

Kwak WJ, Jung HG, Lee SH, Park JB, Aurbach D, Sun YK (2016) Silver nanowires as catalytic cathodes for stabilizing lithium-oxygen batteries. J Power Sources 311:49–56

Lee HL, Chang WJ (2011) Surface effects on axial buckling of nonuniform nanowires using non-local elasticity theory. Micro Nano Lett IET 6:19–21

Li Y, Song J, Fang B, Zhang J (2011) Surface effects on the postbuckling of nanowires. J Phys D Appl Phys 44:425304

Li D, Wu GS, Wang W, Wang YD, Liu D, Zhang DC, Chen YF, Peterson GP, Yang R (2012a) Enhancing flow boiling heat transfer in microchannels for thermal management with monolithically-integrated silicon nanowires. Nano Lett 12:3385–3390

Li Y, Chen C, Fang B, Zhang J, Song J (2012b) Postbuckling of piezoelectric nanobeams with surface effects. Int J Appl Mech 4:1250018

Lin H, Li MX, Liu F, Mihailovi D (2014) Amplified ultraviolet detection of natural DNA based on $Mo_6S_{9-x}I_x$ nanowires. Chin Chem Lett 25:645–648

Liu WK, Chen Y (1995) Wavelet and multiple scale reproducing kernel methods. Int J Numer Methods Fluids 21:901–931

Liu WK, Jun S (1998) Multiple-scale reproducing kernel particle methods for large deformation problems. Int J Numer Methods Eng 41:1339–1362

Liu WK, Jun S, Zhang YF (1995a) Reproducing kernel particle methods. Int J Numer Methods Fluids 20:1081–1106

Liu WK, Jun S, Li S, Adee J, Belytschko T (1995b) Reproducing kernel particle methods for structural dynamics. Int J Numer Methods Eng 38:1655–1679

Lu MC, Chen R, Srinivasan V, Carey VP, Majumdar A (2011) Critical heat flux of pool boiling on Si nanowire array-coated surfaces. Int J Heat Mass Transf 54:5359–5367

Matyjaszewski K, Tsarevsky NV (2009) Nanostructured functional materials prepared by atom transfer radical polymerization. Nat Chem 1:276–288

Mousavi H, Khodadadi J, Grabowski M (2015) Electronic properties of long DNA nanowires in dry and wet conditions. Solid State Commun 222:42–48

Nunes D, Calmeiro TR, Nandy S, Pinto JV, Pimentel A, Barquinha P, Carvalho PA, Walmsley JC, Fortunato E, Martins R (2016) Charging effects and surface potential variations of Cu-based nanowires. Thin Solid Films 601:45–53

Park HS (2012) Surface stress effects on the critical buckling strains of silicon nanowires. Comput Mater Sci 51:396–401

Patton ST, Zabinski JS (2005) Fundamental studies of Au contacts in MEMS RF switches. Tribol Lett 18:215–230

Pop E, Sinha S, Goodson KE (2006) Heat generation and transport in nanometer-scale transistors. Proc IEEE 94:1587–1601

Ruffino F, Torrisi V, Grimaldi MG (2015) Twinned Si nanowires grown by high temperature annealing of Au/Si system in vacuum. Superlatt Microstruct 85:592–598

Schelling PK, Shi L, Goodson KE (2005) Managing heat for electronics. Mater Today 8:30–35

Shahba A, Rajasekaran S (2012) Free vibration and stability of tapered Euler–Bernoulli beams made of axially functionally graded materials. Appl Math Modell 36:3094–3111

Shi L, Yu C, Zhou J (2005) Thermal characterization and sensor applications of one-dimensional nanostructures employing microelectromechanical systems. J Phys Chem B 109:22102–22111

Simsek M, Yurtcu HH (2013) Analytical solutions for bending and buckling of functionally graded nanobeams based on the nonlocal Timoshenko beam theory. Compos Struct 97:378–386

Srivastava P, Kumar A, Jaiswal NK (2016) Structural, electronic, and magnetic properties of Mn-doped InP nanowire. Superlatt Microstruct 92:134–142

Tang H, Zhou Z, Bowland CC, Sodano HA (2015) Synthesis of calcium copper titanate ($CaCu_3Ti_4O_{12}$) nanowires with insulating SiO_2 barrier for low loss high dielectric constant nanocomposites. Nano Energy 17:302–307

Tao R, Ardila G, Montes L, Mouis M (2015) Modeling of semiconducting piezoelectric nanowires for mechanical energy harvesting and mechanical sensing. Nano Energy 14:62–76

Wagner GJ, Liu WK (2000) Application of essential boundary conditions in mesh-free methods: a corrected collocation method. Int J Numer Methods Eng 47:1367–1379

Wang GF, Feng XQ (2009) Surface effects on buckling of nanowires under uniaxial compression. Appl Phys Lett 94:141913

Wang GF, Feng XQ (2010) Effect of surface stresses on the vibration and buckling of piezoelectric nanowires. Europhys Lett 91:56007

Wang X, Liu WK (2004) Extended immersed boundary method using FEM and RKPM. Comput Methods Appl Mech Eng 193:1305–1321

Wang KF, Wang BL (2011) Combining effects of surface energy and non-local elasticity on the buckling of nanoplates. Micro Nano Lett IET 6:941–943

Wang GF, Yang F (2011) Postbuckling analysis of nanowires with surface effects. J Appl Phys 109:063535

Wang X, Song J, Liu J, Wang ZL (2007) Direct-current nanogenerator driven by ultrasonic waves. Science 316:102–105

Xiao J, Ryu SY, Huang Y, Hwang KC, Paik U, Rogers JA (2010) Mechanics of nanowire/nanotube in-surface buckling on elastomeric substrates. Nanotechnology 21:085708

Xu S, Hansen BJ, Wang ZL (2010) Piezoelectric-nanowire-enabled power source for driving wireless microelectronics. Nat Commun 1:93

Yang L, Luo S, Liu S, Cai Q (2008) Graphitized carbon nanotubes formed in TiO_2 nanotube arrays: a novel functional material with tube-in-tube nanostructure. J Phys Chem C 112:8939–8943

Zhu G, Yang R, Wang S, Wang ZL (2010) Flexible high-output nanogenerator based on lateral ZnO nanowire array. Nano Lett 10:3151–3155